EUR 3759 e

EUROPEAN ATOMIC ENERGY COMMUNITY - EURATOM

PHASE AND VELOCITY DISTRIBUTION IN TWO-PHASE ADIABATIC ANNULAR DISPERSED FLOW

by

P. ALIA, L. CRAVAROLO,
A. HASSID and E. PEDROCCHI
(CISE)

1968

EURATOM/US Agreement for Cooperation

EURAEC Report No. 1091 prepared by CISE
Centro Informazioni Studi Esperienze, Segrate (Milan) - Italy

Euratom Contract No. 060-61-7 RDI

LEGAL NOTICE

This document was prepared under the sponsorship of the Commission of the European Communities in pursuance of the joint programme laid down by the Agreement for Cooperation signed on 8 November 1958 between the Government of the United States of America and the European Communities.

It is specified that neither the Commission of the European Communities, nor the Government of the United States, their contractors or any person acting on their behalf :

Make any warranty or representation, express or implied, with respect to the accuracy, completeness, or usefulness of the information contained in this document, or that the use of any information, apparatus, method, or process disclosed in this document may not infringe privately owned rights; or

Assume any liability with respect to the use of, or for damages resulting from the use of any information, apparatus, method or process disclosed in this document.

This report is on sale at the addresses listed on cover page 4

at the price of FF 12.50	FB 125.—	DM 10.—	Lit. 1560	Fl. 9.—

When ordering, please quote the EUR number and the title, which are indicated on the cover of each report.

Printed by Guyot, s.a.
Brussels, March 1968

This document was reproduced on the basis of the best available copy.

EUR 3759 e

PHASE AND VELOCITY DISTRIBUTION IN TWO-PHASE ADIABATIC ANNULAR DISPERSED FLOW
by P. ALIA, L. CRAVAROLO, A. HASSID and E. PEDROCCHI (CISE)

European Atomic Energy Community - EURATOM
EURATOM/US Agreement for Cooperation
EURAEC Report No. 1091 prepared by CISE
Centro Informazioni Studi Esperienze, Segrate (Milan) - Italy
Euratom Contract No. 060-61-7 RDI
Brussels, March 1968 - 86 Pages - 35 Figures - FB 125

In the so-called annular-dispersed regime, the two-phase (gas + liquid) flow can be characterized by two main regions. In the first region (called "core"), located in the central part of the duct, the gas is the continuous phase while the liquid flows in the form of small droplets. In the second region, located close to the wall of the duct, the liquid is the continuous phase.

This report presents and discusses the phase distribution and velocity profiles in this regime, as they have been measured at CISE.

EUR 3759 e

PHASE AND VELOCITY DISTRIBUTION IN TWO-PHASE ADIABATIC ANNULAR DISPERSED FLOW
by P. ALIA, L. CRAVAROLO, A. HASSID and E. PEDROCCHI (CISE)

European Atomic Energy Community - EURATOM
EURATOM/US Agreement for Cooperation
EURAEC Report No. 1091 prepared by CISE
Centro Informazioni Studi Esperienze, Segrate (Milan) - Italy
Euratom Contract No. 060-61-7 RDI
Brussels, March 1968 - 86 Pages - 35 Figures - FB 125

In the so-called annular-dispersed regime, the two-phase (gas + liquid) flow can be characterized by two main regions. In the first region (called "core"), located in the central part of the duct, the gas is the continuous phase while the liquid flows in the form of small droplets. In the second region, located close to the wall of the duct, the liquid is the continuous phase.

This report presents and discusses the phase distribution and velocity profiles in this regime, as they have been measured at CISE.

Phase and velocity distribution in the core was determined by means of a probe which could operate either as a Pitot probe or as an isokinetic sampling probe. In the region close to the wall, the flow rates distribution was determined by means of a suitably-shaped isokinetic sampling probe. Thickness data of the "film region" have been also taken through an electrical method.

The experiments were carried out at high pressure (up to $\sim$ 22 kg/cm^2 abs.) and room temperature with argon-water and argon-ethyl alcohol mixtures in adiabatic vertical upward flow in circular tubes (1.5 and 2.5 cm I.D.). The measurements were performed in a position 3.5 m far from the mixing section. At this position, the flow was found to be fully (or almost fully, in the case of the highest flow rates) developed.

Phase and velocity distribution in the core was determined by means of a probe which could operate either as a Pitot probe or as an isokinetic sampling probe. In the region close to the wall, the flow rates distribution was determined by means of a suitably-shaped isokinetic sampling probe. Thickness data of the "film region" have been also taken through an electrical method.

The experiments were carried out at high pressure (up to $\sim$ 22 kg/cm^2 abs.) and room temperature with argon-water and argon-ethyl alcohol mixtures in adiabatic vertical upward flow in circular tubes (1.5 and 2.5 cm I.D.). The measurements were performed in a position 3.5 m far from the mixing section. At this position, the flow was found to be fully (or almost fully, in the case of the highest flow rates) developed.

EUR 3759 e

EUROPEAN ATOMIC ENERGY COMMUNITY - EURATOM

PHASE AND VELOCITY DISTRIBUTION IN TWO-PHASE ADIABATIC ANNULAR DISPERSED FLOW

by

P. ALIA, L. CRAVAROLO,
A. HASSID and E. PEDROCCHI
(CISE)

1968

EURATOM/US Agreement for Cooperation

EURAEC Report No. 1091 prepared by CISE
Centro Informazioni Studi Esperienze, Segrate (Milan) - Italy

Euratom Contract No. 060-61-7 RDI

SUMMARY

In the so-called annular-dispersed regime, the two-phase (gas + liquid) flow can be characterized by two main regions. In the first region (called "core"), located in the central part of the duct, the gas is the continuous phase while the liquid flows in the form of small droplets. In the second region, located close to the wall of the duct, the liquid is the continuous phase.

This report presents and discusses the phase distribution and velocity profiles in this regime, as they have been measured at CISE.

Phase and velocity distribution in the core was determined by means of a probe which could operate either as a Pitot probe or as an isokinetic sampling probe. In the region close to the wall, the flow rates distribution was determined by means of a suitably-shaped isokinetic sampling probe. Thickness data of the "film region" have been also taken through an electrical method.

The experiments were carried out at high pressure (up to $\sim$ 22 kg/cm^2 abs.) and room temperature with argon-water and argon-ethyl alcohol mixtures in adiabatic vertical upward flow in circular tubes (1.5 and 2.5 cm I.D.). The measurements were performed in a position 3.5 m far from the mixing section. At this position, the flow was found to be fully (or almost fully, in the case of the highest flow rates) developed.

KEYWORDS

TWO-PHASE FLOW
GAS FLOW
LIQUID FLOW
TUBES
DROPLETS
VELOCITY
CONFIGURATION
PITOT TUBES
INSTRUMENTS
PRESSURE
ARGON
WATER
ETHANOL
ADIABATIC PROCESSES

TABLE OF CONTENTS

Foreword

This is the eleventh technical report issued by CISE and devoted to the experimental work performed under the CAN-2 Research Program on the hydrodynamics of two-phase adiabatic flow. It presents and discusses the results of the experiments on phase and velocity distribution in two-phase adiabatic annular dispersed flow.

The reports so far issued were devoted respectively to the following subjects:

- CISE R-59: design and construction of a high pressure gas circulator for the new experimental facility.
- CISE R-53: pressure drop and film thickness data obtained with different channel geometries.
- CISE R-73: influence of some physical properties on pressure drop and film thickness.
- CISE R-75: design, construction and assembly of a high pressure experimental facility.
- CISE R-89: development of a new instrument for the investigation of the phase and velocity distribution in the region close to the wall.
- CISE R-82: development of a new instrument for the measurement of shear stress on the wall of a conduit and its application in mean density determination in two-phase flow.
- CISE R-92: development of a method for the measurement of the liquid volume fraction of two-phase two-component mixtures.
- CISE R-93: effect of entrance conditions and length on some hydrodynamics parameters.
- CISE R-105: liquid volume fraction in two-phase adiabatic flow.
- CISE R-110: some spacer effects in annular and cluster geometries in annular dispersed flow.

Work on the hydrodynamics of two-phase flow was also carried out under the previous Research Program CAN-1: the results were presented and discussed in four topical reports (CISE R-26, R-35, R-41 and R-43) and in a special CISE Report ("A Research Program in Two-Phase Flow").

Acknowledgements

The authors wish to thank Prof. M. Silvestri for his useful criticism. They are also indebted to Mr. A. Colombo for his substantial contribution throughout the experimental work.

1. INTRODUCTION

1.1. It is well known that many more flow patterns exist in two-phase flow than in single-phase flow. Without attempting here to distinguish and describe these various patterns (which however may be quite vaguely defined) we shall limit our attention to only one of them, the so-called annular-dispersed flow.

For this type of flow pattern a definition slightly different from that commonly used up to now is necessary. We shall state that annular-dispersed flow is characterized by a continuous gas phase and a discontinuous liquid phase in the central region of the duct, which will be called "core", while just the opposite condition exists in the so called "film" region, close to the wall. In fact, as explained below, recent experiments showed that the gas volume fraction in the region where the liquid is the continuous phase may be quite large and therefore the assumption that the film region is entirely occupied by the liquid phase is no longer valid.

The most important quantities characterizing the hydrodynamics of annular dispersed flow, in fully developed conditions, are: linear gas and liquid velocity (U_g and U_l) distribution, liquid (or gas) volume fraction ($1-\alpha$ or α) distribution. Other interesting quantities of an integral nature are: pressure drop ($\Delta p/\Delta Z$), shear stress on the wall (τ_w), overall density ($\bar{\rho}$), overall slip ratio (S) or overall liquid volume fraction ($1-\bar{\alpha}$). In addition, the knowledge of the amount of liquid which is flowing in the "film" region may be quite useful for its implication in the understanding of heat transfer phenomena. All these quantities depend on flowrates, on the physical properties of both phases and on geometry.

1.2. The experimental study presented here was carried out under the CAN-2 Research Program on the hydrodynamics of two-phase (gas-liquid) flow and was aimed at measuring the velocity and phase distribution profiles over a cross section in annular-dispersed flow.

Work on the same subject was undertaken previously under the CAN-1 Program and the main results of this investigation were presented in a spe-

---

Manuscript received on January 22, 1968

cial CISE Report[1]. The experiments were performed in adiabatic conditions with a two-phase (argon + water) mixture flowing vertically upwards in a circular tube 2.5 cm I.D.; the operating pressure (~22 kg/cm^2 abs) was selected in such a way that the gas density was equal to that of saturated steam at 70 kg/cm^2 abs. The measured quantities were phase and velocity distribution in the core region of annular dispersed flow and the measurements were carried out by means of an isokinetic sampling probe moveable along a diameter which could be operated also as a Pitot probe; the probe was located approximately 1 m from the mixing section and the resulting velocity and phase distribution profiles were found to be strongly assymetrical. In addition, measurements have been taken of the thickness of the liquid film climbing over the wall.

The experimental study described in the present report is the natural development of the work undertaken previously under the CAN-1 Program: its aim was to get a set of systematic experiments over a cross section where the flow configuration could be assumed as that corresponding to fully developmed flow. For this purpose an investigation[2] has been made on the behaviour along length on a longer test section than that available under the CAN-1 Program (3.5 m against 1.5 m)[3].

The aim of the present investigation was also to get a better knowledge of the phase and velocity distribution in the "film region" and in particular to determine the liquid flow rate in that region, a parameter of primary importance for the understanding of heat transfer in annular-dispersed flow. A special probe was therefore devised for this purpose.

1.3. The experimental studies described here were initiated at the beganning of 1962 and were continued at intervals during a period of about 18 months.

At the beginning very few similar studies could be found. Extensive investigations were available with air-water mixtures at atmospheric pressure [5] [6] [7] [8]; since then, however extensive investigations have been published on phase and velocity distribution both in the film and in the "core" region[(°)].

(°) An exhaustive review on the subject has recently been made by Collier and Hewitt[9].

However, even at present, the available data with two-phase miwtures are very limited (at high pressure): this is due to the difficulties and the time needed for carrying out such measurements, which is very large. Perform ing experiments at high pressure is of the utmost importance: gas density in fact plays quite an important role on the hydrodynamics behaviour of the two phase flow (see for example [12] where the influence of gas density on the "thickness" of the film region has been brought out).

Simultaneously with the present experiments and on the basis of the results of the present investigation, measurements have been made with steam-water mixtures both in adiabatic conditions and with heat addition[10]. The results of these experiments are in good agreement with those obtained with two component mixtures in the present investigation.

2. EXPERIMENTAL

2.1. The experiments were carried out with the experimental facility already installed at CISE for studying the hydrodynamics of two-phase (gas+liquid) mixtures in adiabatic flow. A schematic flow sheet of the circuit, which has been described in detail in ref.[3], is given in fig. 1.

The two-phase miwture is formed in a tee-mixer with the gas entering the run side; the liquid is injected through an annular slot with an adjustable aperture[+]. After passing through a calming section (50 cm long) the mixture enters the vertical test section. At the top, the test section leads into a high efficiency separator, consisting of three different devices in series, from which each separated phase returns to its own circuit.

2.2. As stated, the measured quantities are:

- thickness (s) of the film adhering to the wall over a given length of the test section;
- phase and velocity distribution profile along a cross section diameter.

The value of the thickness[1] (the so-called "electric film thickness") has benn derived from the measurement of the electrical resistance of the liquid layer over a given length of the test section (made of an insulating material) as well as of the resistivity of the circulating liquid.

The phase and velocity distribution was measured by means of two different sampling probes. In the central region (up to 2 mm from the wall) a small cylindrical sampling probe was used[1]: it was operated in turn as an isokinetic probe[°] (thus giving the local specific mass flow rate of both phases G_l and G_g) and as a Pitot tube (thus giving the impact pressure P_p).

(+) The aperture was fixed at 2.77 mm for all the experiments.

(°) A sampling is said to be isokinetic when the conditions at the inlet of the probe are the same as the pre-existing ones.

Making certain assumptions on the behaviour[1] of a Pitot tube in two-phase flow, the following equation was derived for the local value of $1 - \alpha$:

$$1 - \alpha = \frac{2}{\frac{2 \Delta P_p \rho_l}{G_l^2} + 1 - \left(\frac{G_g}{G_l}\right)^2 \frac{\rho_l}{\rho_g}}$$

where ΔP_p is the impact pressure. Local velocity of the two phases and local liquid (or gas) volume fraction, may thus be computed from the measured quantities by utilizing the above relationship.

The sampling probe used in the present experiments is similar to the probe N. 2 employed previously[1]: a schematic drawing, showing the main dimensions, is reported in fig. 2. The device for the introduction and positioning of the probe was completely re-designed with respect to that used in [1]: the new device (figs. 3 and 4)[2] gives a much higher accuracy in the radial position and considerably reduces the time needed for the measurements.

In the region close to the wall (from 0.13 mm up to 2 mm from the wall) a suitably shaped (figs. 5,6,7) sampling probe was used, which has been exhaustively described in [4]; it was always operated as an isokinetic probe (see footnote page 4). This probe gives the integrated flow rate between the wall and a distance variable at will: in this region the local slip ratio was always supposed to be unity(°) and therefore the local volume fraction may be strainght-forwardly computed from the local flow rates.

The errors inherent in the measurement methods have been discussed in detail in[1] and [4]. As far as the phase distribution and velocity profiles are concerned the following remarks can be made:

- The reliability of the two probes and of the measurement procedure was checked by performing special experiments with single phase (gas) flow.

(°) This appeared reasonable in view of the small size of the gas bubbles likely to be present in the film region (3.2) and also because in bubble flow the slip ratio is very close to unity.

The total flow rates obtained through an integration process from the velocity profiles Γ_g^i are compared to the orifice readings Γ_g in table I. As shown, the maximum deviation from the orifice reading for the experiments with isokinetic sampling probe is 6% while must of the results lie within $\pm$ 2%, which is the orifice accuracy. As for the experiments with the Pitot probe, at least for one point for each profile a check was made that the reading was equal, within the experimental inaccuracy, with the isokinetic sampling datum; moreover for one profile a check was made that the integrated mass flow rate would agree with the orifice reading (Table I).

- An idea of the accuracy of the local values of liquid and gas specific mass flow rates with two-phase flow can be given, as in the single phase flow case, by a comparison between the integrated values of both flow rate distributions and the orifice readings. Such a comparison is made in table II. Although the agreement between the two sets of values (on the average $\pm$ 10% for both phases) is worse than in the case of single - phase flow, it can be considered still satisfactory.

  From this comparison the conclusion can be inferred that, at least the G_g and G_l distribution profiles are accurate within $\pm$ 10% on the average.

- The local values of liquid volume fraction (and any related quantity) are affected by the inherent unknown inaccuracy of the relationship linking $1-\alpha$ to ΔP_p, G_l and G_g. Ref. (1) has demonstrated that the error inherent in the $1-\alpha$ values can be quite large (10 to 50%)). To get a rough idea of this error a comparison was also made between the values integrated from the $1-\alpha$ profiles, and the experimental values of $1-\bar{\alpha}$ obtained directly from the liquid level method[14]. As shown in table III the agreement between the two sets of values is on the average within 10% (in general the $1-\alpha$ values derived from the integration of the profiles are slightly lower than the other ones; this might be due to the fact the local slip ratios derived from the said relationship are actually relatively larger or that the $1-\alpha$ values obtained with the liquid level method are higher; this could be possible since these data are overall data relevant to the whole test section and it has been observed that $1-\alpha$ undergoes a decrease along flow direction (11).

2.3. The experiments were performed with argon-water and argon-ethyl alcohol mixtures at various gas densities(+) in order to investigate the influence of the two physical properties (gas density and surface tension(°)) which have been observed to have most influence on the two-phase flow behaviour[12]. The physical properties of these mixtures are indicated in table IV.

Temperature of the test section was between 18 and 20 °C.

Two circular conduits were experimented, 2.5 cm I.D. and 1.5 cm I.D. (with 1.5 cm I.D. element only film thickness measurement have been made).

The investigated range of flowrates is reported in table V.

Assuming a symmetry around the axis of the duct, the problem still remains of determining whether the flow is fully developed, that is the measured quantities are independent of the axial coordinate. This aspect was throughtly investigated under previous special tests[2]: the systematic measurements described here were always performed so far from the two phase mixer (~3.5 m) that axial (or memory) effects were either negligible or minimized, as the tests have shown.

2.4. The experimental results are given in tables VI, VII, VIII for the film thickness experiments and in the table IX to XXV as far as phase distribution and velocity profiles are concerned.

In tables VI, VII and VIII the following quantities have been reported:

$\bar{G}_g$: average gas specific mass flowrate (= gas flowrate divided by the tube cross section area) (g/cm^2s)

$\bar{G}_l$: average liquid specific mass flow rate (= liquid flowrate divided by the tube cross section area) (g/cm^2s)

s : electrical film thickness[1] (cm)

In tables IX to XXV the following quantities have been reported:

(+) The experiments at various gas densities were carried out at the same volume flow rate due to the blower characteristics[3] which do not allow operation at constant mass flow rate.

(°) With argon-ethyl alcohol mixtures film thickness could not be measured due to the liquid conductivity being too low.

y : distance from the conduit wall (cm). For the experimental points obtained with the film sampling probe (signed with $^{(+)}$ in the y column) the distance y corresponds to the average between two adjacent values of the probe position. For the core sampling probe experiments y indicates the distance from the wall of the centre of the probe

y' : distance from the conduit wall (cm) (only for the film sampling probe position

ΔP_p : impact pressure (as from Pitot probe readings) (dyn/cm^2)

G_g : local gas specific mass flowrate (= gas sampling flowrate divided by the probe cross section area) (g/cm^2s)

G_l : local liquid specific mass flowrate (= liquid sampling flowrate divided by the probe cross section area) (g/cm^2s)

$1-\alpha$: local liquid volume fraction

S : slip ratio (only for the measurements with the core sampling probe)

Γ_l : liquid flowrate in the annular area comprised between the conduit wall and the circumference having a radius = R - y'

Γ_g : gas flowrate in the annular area comprised between the conduit wall and the circumference having a radius = R - y'.

The experimental results are also given in the form of diagrams: film thickness measurements are reported in figs. 8,9 and 10 while phase distribution and velocity profiles are given in figs. 11 to 27.

3. GENERAL RESULTS

A typical diagram of the local values of some measured quantities over a cross section as a function of the radial coordinate is shown in fig. 28, to which reference is made throughout this paragraph unless otherwise stated.

3.1. The liquid volume fraction distribution has a minimum in the center of the duct: this was found over the whole range of flow rates and physical properties investigated, provided the flow pattern is annular-dispersed. From this minimum the value of $1-\alpha$ increases going toward the wall and reaches unity in a region comprised between $y = 0$ and $y = 0.13$ mm, which is our instrument limitation. No discontinuity is revealed along the radial coordinate even at the core film interface. Flattening of the $1-\alpha$ profile, with which a higher degree of dispersion is believed to be associated, depends on the magnitude of the flow rates and on the physical properties of both phases.

3.2. As expected from the shape of the $1-\alpha$ profile the local value of the liquid specific mass flow rate G_l also has a minimum on the conduit axis and increases toward the wall. The trend however is not always monotonous and a relative minimum may exist not far from the "film" region. The maximum value of G_l is always very close to the wall and well inside the "film" region. At the wall G_l is always supposed to be zero.

Similar qualitative results were observed by authors, at least in the core region [1][7][8]. The British team at Harwell[15], however, operating with air-water mixtures at nearly atmospheric pressure, found that the G_l profile given flatter and flatter when increasing the distance from the entrance until an inversion appeared with a relative maximum on the conduit axis. The consequence in this case is that the $1-\alpha$ profile is almost flat in the whole core region.

As stated, all the present measurements were performed at 3.5 m from the entrance. At this distance the Harwell experiments already show a convexity in the G_l profile. As has already been examined by Hewitt[16] and

discussed in a previous CISE Report[2], a number of reasons explaining such a discrepancy can be invoked, for example:

1) difference in gas velocity: the average gas velocity (20-30 m/s) beyond which the Harwell team found a change in concavity is in general higher than the average gas velocity of the present experiments. This, however, is in contrast with the profile reported in fig. 16, which has been taken at 3.5 m from the entrance and to which a gas velocity equal to 37 m/s corresponds.

2) difference in gas density: the different gas density (and gas compressibility) in the two sets of experiments could play an important role either because the rate of progress towards equilibrium is different or because it is practically impossible, as stated, to distinguish the effect intrinsic to the mixture from the effect due to the gas density variation along flow direction. The effect of gas density has been investigated, at least to a certain extent, with argon-water mixture (par. 3.4) at a gas density equal to $\rho_g = 10.0 \times 10^{-3}$ g/cm^3 and with the following flow rate combination:

$$\bar{G}_g = 22.6 \text{ g/cm}^2\text{s} \qquad \bar{G}_l = 91 \text{ g/cm}^2\text{s}$$

As shown in Fig. 21, the results are almost identical (at the same gas velocity approximately) to that obtained at $\rho_g = 36.1 \times 10^{-3}$ g/cm^3, i.e. the G_l profile has a concavity that is always directed upwards.
This, however, is not enough to exclude the difference in gas density as the reason for the discrepancy, since (i) the gas density investigated is still much larger than that of air at atmospheric pressure, (ii) the gas velocity is lower than the aforesaid limit of 20-30 m/s, and (iii) the pressure drop is still negligible in comparison with the operating pressure.

3) difference in length: the available length of the Harwell test element is about 30% larger than the one available in the facility referred to in this report. This however should be only a minor effect since the change in concavity is much lower than the length investigated here.
In addition to these remarks it must be observed that the liquid flow rates covered in our experiments are larger than those experience at Harwell[5]. According to the observations of that Laboratory, the change

in shape of the G_l profile is the more pronounced the larger G_l. In our case therefore, there is more reason to observe such a change.

In conclusion, since, as stated previously, the experiments reported here indicate that at the top of the test section, the flow configuration is quite close to the fully developed one, the discrepancy between the two results should be ascribed mainly to the different operating pressure and, therefore, to the gas density. In any case the question still remains open: in order to get a definite answer, it would be necessary to carry out experiments with longer test sections, varying the inlet conditions so drastically as to realize at the entrance, for a given flow rate combination, quite different flow configurations. The experiments should be of course carried out at high pressure so as to minimize the gas density variations along flow direction(+).

3.3. Gas velocity profiles (U_g) are similar to those found in single phase flow: usually, however, they are steeper, depending on the value of flow rates and physical properties of both phases. Both roughness due to the irregularities at the core-film interface and damping of turbulence by liquid droplets could contribute to this phenomenon.

3.4. Local values of the slip ratio were measured only in the core region: they range between 1 and 1.6 with a slight tendency to increase toward the wall. If the hypothesis is made that S is unity very close to the wall (see 1.1), its value must go through a maximum at the liquid gas interface.

The local values of slip ratio in the central region decreases with increasing gas density (at constant volume flow rate) as well as with decreasing surface tension, i.e. the flow has a tendency to become locally more homogeneous.

(+) Another interesting difference between the results obtained at CISE and Harwell is that, while in our case the whole flow pattern is involved in the variation along flow direction (both liquid film thickness and entrained liquid profiles change along the flow direction), in the Harwell experiments each of the two regions seems to behave on its own. Film thickness in fact does not vary, while, inside the core, the entrained liquid increases in the centre to the detriment of the region of the core close to the film region.

On the whole, it can be inferred from the low values of slip ratio which have been measured, that the assumption of a locally homogeneous flow is not unreasonable.

4. PHASE AND VELOCITY DISTRIBUTION CLOSE TO THE WALL

4.1. Reference is made to fig. 29 where the local values of the ratio $U_g/\bar{U}_g^* = G_g^*/\bar{G}_g^* = G_g/\alpha \Big/ \bar{G}_g/\bar{\alpha}$ for a single typical case is reported. From this diagram it appears that the curve has somewhat a regular trend on both sides of a region located around the electrical film thickness both in the core and in the film region. In quantitative terms this appears to be true for $y \tilde{<} s/2$ and $y \tilde{>} 2\ s$; while for $s/2 < y < 2\ s$, $U_g/\bar{U}_g^*$ presents an ambigous trend. Actually this might correspond to an ambigous trend aither of $U_g/\bar{U}_g^*$, or of the slip ratio which, in this region, ought to be assumed to be equal to one (see 2.1.). This set-up, which is evident in most cases, disappears for low mass flow rates and gas density; moreover, with liquids having low surface tension (ethyl alcohol), for some unknown reason, the inflection region appears further inside the electrical film.

Another phenomenon, which was always observed, was a maximum in the $G_l/\bar{G}_l$ diagram (fig. 29), approximately at a distance from the wall corresponding to s/2. This maximum, the shape of which depends on the physical conditions (flow rates and physical properties), is believed to be related to a steep increase of the gas volume fraction at a distance larger then s/2.

This fact, together with what was said above the U_g/U_g^* trend between s/2 and 2 s, seems to confirm the assumption that in this region a transition takes place between the "film" and the "core" regions. Moreover, it is reasonable to presume that most of the waves which set up at the film-core interface (which have been extensively investigated by other researchers) are confined in this region: this is not in contrast with what has been observed elsewhere[17].

4.2. The value of $1-\alpha$ in the region close to the wall (derived through the assumption that the local slip ratio is equal to one (par. 22), decreases, monotonously from unity at the wall (or, at least, in the uninvestigated region where $y \leq 0.13$ mm) to about 0.6 ÷ 0.8 in correspondence with the maximum of G_l and 0.3 ÷ 0.5 at the electrical film thickness. Then, the liquid volume fraction decreases toward the center (with water always and

with alcohol at low G_g values), or, for alcohol at high G_g values, reaches a relative maximum before decreasing again towards the center.

As a consequence, the overall gas volume fraction in the "film" region can be rather high: up to y = s this value ranges between 0.2 and 0.5, with a tendency to increase with increasing flow rates. The assumption that $1-\alpha = 1$ up to y = s in order to evaluate the density of the mixture (1.2) from the values of s and the phase distribution in the core[1] can therefore largely overstimate (about 10+20%) this quantity.

The large values of α that are found well inside the film region, cannot be explained merely by the wavy nature of the film-core interface, but it must be imagined that in this region the gas phase is present in the form of small bubbles. In the light of this consideration, also taking into account the fact that a profile configuration and not just a number would be necessary to individuate the core-film interface, the realtionship between the electrical film thickness and the actual extension of the region in which the liquid is the continuous phase cannot be established. The usefulness of the determination of s, however, does not lose all its value, in our opinion, since it still gives an idea of the extension of the film region.

4.3. A parameter of interest, also for its connection with the heat transfer capability of two phase flow, is the amount of liquid which flows along the wall in the "film" region (which has been investigated with the film probe).

In single phase flow the ratio $\Gamma_y/\pi D \mu$, where Γ_y is the mass flow rate up to the distance y from the wall, in circular conduits, is given by:

$$\frac{\Gamma_y}{\pi D \mu} = f\,(y^+, Re^+) \qquad (1)$$

where

$$y^+ = \frac{y}{\mu}\ \tau_w \rho$$

$$R_e^+ = \frac{\rho U^+ D}{\mu}\ ;\quad U^+ = \frac{\sqrt{\tau_w}}{\rho}$$

In plane geometry, or in circular geometry when $\frac{y}{R} << 1$, $\frac{y}{D}$ becomes a function of y^+ only, so that:

$$\Gamma_y = \pi D \mu \quad f(y^+) \tag{2}$$

To check the validity of this formula in two-phase flow, the ratio $\frac{\Gamma_{ly}}{\pi D \mu_l}$ was plotted (fig. 30) against y^+ (where $y^+ = \frac{y}{\mu_l} \sqrt{\tau_w \rho_l}$) for all the profile investigated, i.e. for argon-water and argon-alcohol mixtures at two gas densities. Apparently, also in two-phase flow up to $y^+ \simeq s^+$ the ratio $\frac{\Gamma_{ly}}{\pi D \mu_l}$ is a function of y^+ only, although different from single-phase flow. Beyond this value $\frac{\Gamma_{ly}}{\pi D \mu_l}$ has in general a tendency to be lower than the value expected following the correlation valid for $y^+ \leq s^+$.

Since, for the reasons stated above, a true film region cannot be well defined from our experimental results, the correlation between $\frac{\Gamma_{ly}}{\pi D \mu_l}$ and y^+ is not enough to give the "film" flow rate. However, as a first approximation, just to have an idea of the magnitude of this quantity and of its dependence on the physical properties and flow rates, one can assume as "film" flow rate the liquid flow rate (Γ_F) measured up to y = s. In the light of previous considerations (4.2), this value should not be very different from the actual "film" flow rate. The results, for all the investigated conditions, are presented in fig. 31 where the ratio $\frac{\Gamma_F}{\pi D \mu_l}$ is reported against $s^+ = \frac{s}{\mu_l} \sqrt{\tau_w \rho_l}$ on a log-log chart. This ratio seems to be well correlated to s^+ (for $30 \leq s^+ \leq 300$) through the equation:

$$\frac{\Gamma_F}{\pi D \mu_l} = 5.3 \, (s^+)^{1.1} \tag{3}$$

The constant 5.3 and the exponent 1.1 seem to be independent of the flow-rates and the physical properties investigated (gas density, surface tension and, to a certain extent, liquid density and viscosity).

Equation (3) is quite a simple relationship which allows, within the approximation of the above assumption, the determination of Γ_F once s and τ_w are known. It must be kept in mind, however, that nothing can be said about the influence of the diameter of the conduit on the film flow rate since this variable was not investigated. The presence of D in eq. (3) could not therefore represent the actual dependence on D.

For the above-stated reasons, the core-film interface should be comprised between ~ s/2 and ~ 2 s. If the same plot of fig. 31 is made for these two values, the experimental points become more scattered but the overall trend versus 1/2 s^+ or 2 s^+, that is, the value of the exponent (1.1), is preserved. It may be inferred, therefore, that the dependence of Γ_F on flow rates and physical properties is well represented through the parameter s^+. Of course, this is true only if the ratio between the electrical film thickness and that distance from the wall where Γ_{ly} is equal to the actual "film" liquid flow rate does not depend largely on these parameters.

For purposes of comparison, the same figure shows the quantity $\frac{\Gamma_F}{\pi D \mu_l}$ as evaluated (i) according to the Dukler analysis modified by Hewitt[18] and (ii) assuming as still valid in the film region the velocity profile proposed by von Karman in single phase flow. Since, according to these theories the ratio $\frac{\Gamma_F}{\pi D \mu_l}$ is not a function of y^+ only, two curves are reported which represent the extreme limits within the range investigated. As an average value, the value predicted by these theories are overstimated (40 + 60%) in comparison with the experimental values (for $30 \leq s^+ \leq 300$).

3.6. The dependence of the "film" flow rate (Γ_F), as defined above, on the forced flow rates and on physical properties has been determined from the experimental values of s and τ_w by evaluating this quantity through equation (3).

The ratio Γ_F/Γ_l with argon-water mixtures at $\rho_g = 36.1 \times 10^{-3}$ g/cm^3 is presented in fig. 32 as a function of the mass quality (X) and with the total specific mass flow as a parameter. This ratio, which varies from

0.1 to 0.4, decreases with increases in both G and X.

Since, at constant mass flow rate, the shear stress on the wall was found proportional to $\frac{1}{\rho_g}$ [19] and the electrical film thickness to $\rho_g^{0.55}$ [12], the influence of gas density on s^+, hence on film flow rate, is negligible.

Surface tension, on the contrary, influences this quantity because, as shown by our experimental results, both τ_w [19] and s [12] decrease with it as do s^+ and Γ_F. This effect is more pronounced at high values of mass quality and flowrate.

5. PHASE AND VELOCITY DISTRIBUTION IN THE "CORE" REGION

5.1. In the whole range investigated, the liquid volume fraction in the "core" region always has a minimum in the center of the duct. An analytical expression, however, cannot easily be found and monomial expressions, as that proposed by Bankoff[20], are not satisfactory. A general observation is that the $(1-\alpha)$ profile tends to flatten with:

a) increasing flow rates;

b) increasing gas density at constant volume flow rate;

c) decreasing surface tension.

As the $(1-\alpha)$ profile becomes more flattened, the absolute value in the "core" region increases, which is indirect evidence of a more "dispersed" pattern.

The upward concavity of the $(1-\alpha)$ profile as a function of y still shows that, provided fully-developed flow is established, droplet diffusion is not the predominating mechanism for liquid distribution in the "core" region. Other mechanisms should therefore be called upon and their concepts analytically assessed.

S. Levy, for example, described the phase and velocity distribution analytically, treating the two-phase system as a continuous medium and applying to it the mixing length model widely accepted in single-phase turbulent flow[21]. Although some assumptions made during the development of this theory do not correspond in our cases to the experimental evidence, the predicted values both of the density (or $1-\alpha$) profiles and of the mean density are in rather good agreement with the experimental values, especially at the high gas flow rates. As an example, fig. 33 shows the experimental profile of ρ compared with that computed from the Levy mixing length model, assuming as inlet parameters the values of liquid and gas flow rates and of shear stress on the wall.

Another process which might explain the trend of $1-\alpha$ is that of droplet coalescence, that is of capture of the droplets among themselves, which was proposed previously[1]. The analytical treatment presents, however, serious difficulties.

5.2. As stated earlier, the gas velocity profiles are always less flattened than in single-phase flow, the gas Reynolds number being equal. The higher the gas flow rates the greater the flattening while there is a certain degree of independence on the liquid flow rate. Physical properties, too, have an influence on the shape of the $U_g/\bar{U}_g^*$ profile: as shown in fig. 39 flattening increases with increasing gas density (at constant volume flow rate) and with decreasing surface tension.

The experimental results show that there is a close relationship between the shape of the gas velocity profile and the value of the film thickness, whatever the gas flow rate, gas density and surface tension: film thickness is larger for the steeper profiles. On the other hand, larger film thicknesses would be associated with larger surface waves[17] at the core-film interface corresponding to a greater apparent roughness of the duct in which the gas is flowing. This apparent roughness can therefore be taken to be partly responsible for this effect in single phase flow where a higher degree of roughening is associated, at the same Reynolds number, with steeper velocity profiles.

The assumption that the larger steepness of the gas velocity profiles in two-phase flow is due to the presence of liquid in the "core" region, in the form of small droplets damping the turbulence of the gas flow, seems to be in contrast with the experimental evidence: in fact it was always observed (with varying G_g, ρ_g, γ) that the steeper the profile, the smaller the value of $1-\alpha$ in the central region. However, since an increase of film thickness is always associated with a decrease of $1-\alpha$ in the core, the assumption cannot be excluded a priori.

5.3. In single phase flow, a law representing the velocity profile in the central region of the duct fairly well is the so-called "velocity deficiency law":

$$\frac{U_o - U}{\sqrt{\tau_w/\rho}} = f\,(y/R)^{(\circ)} \qquad (4)$$

(°) U_o is the velocity at the center of the conduit.

A suitable expression of f(y/R), valid both for smooth and rough ducts is the following:

$$f\,(y/R) = 1/k \;\; \ln \frac{R}{y}$$

where k, the von Karman constant, is equal to 0.4.

Almost all the gas velocity profiles(°) determined in two-phase flow obey the same law, as shown in fig. 35 for five particular cases. The numerical values of k is, however, lower ($\sim$0.27 for argon-water mixtures and $\sim$ 0.31 for argon-alcohol mixtures) in agreement with the experimental results obtained elsewhere with air-water mixtures at atmospheric pressure[15]. As a consequence, the mixing length which, as defined in single phase flow, is proportional to k, is also lower: this could be interpreted as a lower degree of turbulence in the "core" region of two-phase dispersed flow.

(°) The value of ρ in eq. 4 was put equal to ρ_g.

Nomenclature

Latin symbols

A	cross sectional area of the test section
D	diameter of the test section
G^*	local mass velocity ($G_g^* = \frac{(\Gamma_g)_s}{\alpha\,\sigma}$; $G_l^* = \frac{(\Gamma_l)_s}{(1-\alpha)\sigma}$)
G	local specific mass flowrate ($G_g = \frac{(\Gamma_g)_s}{\sigma}$; $G_l = \frac{(\Gamma_l)_s}{\sigma}$)
$\bar{G}^*$	average mass velocity ($\bar{G}_g^* = \frac{\Gamma_g}{\bar{\alpha}A}$; $\bar{G}_l^* = \frac{\Gamma_l}{(1-\bar{\alpha})A}$)
$\bar{G}$	average specific mass flowrate ($\bar{G}_g = \frac{\Gamma_g}{A}$; $\bar{G}_l = \frac{\Gamma_l}{A}$)
Q	volume flowrate ($Q_g = \frac{\Gamma_g}{\rho_g}$; $Q_l = \frac{\Gamma_l}{\rho_l}$)
R	radius of the test section
s	electrical film thickness
S	local slip ratio ($S = U_g/U_l$)
$\bar{S}$	overall slip ratio ($S = \bar{U}_g/\bar{U}_l$)
U	local linear velocity ($U_g = \frac{(\Gamma_g)_s}{\alpha\sigma\rho_g}$; $U_l = \frac{(\Gamma_l)_s}{(1-\alpha)\sigma\rho_l}$)
U^*	local superficial velocity ($U_g^* = \frac{(\Gamma_g)_s}{\sigma\rho_g}$; $U_l^* = \frac{(\Gamma_l)_s}{\sigma\rho_l}$
$\bar{U}^*$	average linear velocity ($\bar{U}_g^* = \frac{Q_g}{\bar{\alpha}A}$; $\bar{U}_l^* = \frac{Q_l}{(1-\bar{\alpha})A}$
$\bar{U}$	average superficial velocity ($\bar{U}_g = \frac{Q_l}{A}$; $\bar{U}_l = \frac{Q_l}{A}$)
X	mass flow rate quality (or mass quality) ($X = \frac{\Gamma_g}{\Gamma_g + \Gamma_l}$
X_v	volume flow rate quality ($X_v = \frac{Q_g}{Q_l + Q_g}$)
y	distance from the wall of the conduit

Greek symbols

α	local gas volume fraction
$\bar{\alpha}$	overall gas volume fraction
γ	surface tension
Γ	mass flow rate
μ	viscosity
ρ	local density
σ	cross sectional area of extraction probe inlet
τ_w	shear stress of the wall of the conduit

Subscript

F	film
g	gas
l	liquid
s	probe
tot	total (gas+liquid)

References

1. "A research program in two-phase flow" CISE Report (January 1963).
2. L. Cravarolo, A. Hassid, E. Pedrocchi: "Further investigation on two-phase adiabatic annular-dispersed flow: effect of length and of some inlet conditions on flow parameters". CISE Report R 93 (1964).
3. N. Adorni, L. Cravarolo, A. Giorgini, A. Hassid, E. Pedrocchi: "Design and construction of a high pressure facility for hydrodynamics experiments on two phase flow. Instrumentation. Preliminary tests in single and two-phase flow". CISE Report R 75 (1963).
4. N. Adorni, P. Alia, L. Cravarolo, A. Hassid, E. Pedrocchi: "An isokinetic sampling probe for phase and velocity distribution measurements in two-phase flow near the wall of the conduit". CISE Report R 89 (1963).
5. J.G. Collier, G.F. Hewitt: "Data on the vertical flow of air-water mixtures in the annular and dispersed flow regions. Part II: Film thickness and entrainment data and analysis of pressure drop measurements". Trans. Inst. Chem. Engrs. 39, 127 (1961).
6. M. Wicks, A.E. Dukler: "Entrainment and pressure drop in concurrent gas-liquid flow". A.I.Ch.E. J. 6, 463 (1960).
7. P.G. Magiros, A.E. Dukler: "Entrainment and pressure drop in concurrent gas-liquid flow. II: liquid property and momentum effects". Developments in Mechanics Vol. I, Plenum Press, New York (1961).
8. G.H. Anderson, B.G. Mantzouranis: "Two-phase (gas+liquid) flow phenomena. Liquid entrainment". Chem. Eng. Sci. 4, 12, 233 (1960).
9. J.G. Collier, G.F. Hewitt: "Measurement of liquid entrainment" British Chem. Eng. 11, 11, 1375 (1966).
10. N. Adorni, G. Peterlongo, R. Ravetta, F.A. Tacconi: "Large scale experiments on heat transfer and hydrodynamics with steam-water mixtures: phase and velocity distribution measurements in a round vertical tube" CISE R 91 (1964).
11. P. Alia, L. Cravarolo, A. Hassid, E. Pedrocchi: "Liquid volume fraction in adiabatic two-phase vertical upflow-round conduit" CISE R 105 (1965).

12. L. Casagrande, L. Cravarolo, A. Hassid, E. Pedrocchi: "Adiabatic dispersed two-phase flow: further results on the influence of physical properties on pressure drop and film thickness. CISE R 73 (1963).
13. P. Alia, L. Cravarolo, A. Hassid, E. Pedrocchi, M. Silvestri: "A volume displacement method for measurements on the liquid volume fraction in two-phase adiabatic flow". CISE R 92 (1964).
14. L. Cravarolo, A. Hassid: "Phase and velocity distribution in two-phase adiabatic dispersed flow". Presented at the European Atomic Energy Society Symposium on two-phase flow, steady state burnout and hydrodynamic instability. Studsvik, Sweden, 1st-3rd October, 1963, CISE Report N. 98.
15. L.E. Gill, G.F. Hewitt and J.W. Hitchon: "Sampling probe studies of the gas core in annular two-phase flow". Part I, "The effect of length on phase and velocity distribution" AERE R 3954 (1962).
16. G.E. Hewitt: "Heat transfer and fluid flow in two-phase systems". AERE R 4586 (1964).
17. G.F. Hewitt, R.D. King, P.C. Lovegrove: "Techiniques for liquid film and pressure drop studies in annular two-phase flow" AERE R 3921 (1962).
18. G.F. Hewitt: "Analysis of annular two-phase flow: application of the Dukler analysis to vertical upward flow in a tube" AERE R 3680 (1961).
19. L. Cravarolo, A. Giorgini, A. Hassid, E. Pedrocchi: "A device for the measurement of shear stress on the wall of a conduit. Its application in the mean density determination in two-phase flow. Shear stress data in two-phase adiabatic vertical flow". CISE R 82 (1964).
20. S.G. Bankoff: "A variable density single-fluid model for two-phase flow with particular reference to steam-water flow". Trans. ASME, Journal of Heat Transfer, Nov. 1960.
21. S. Levy: "Prediction of two-phase pressure drop and density distribution from mixing length theory". Trans. ASME, Journal of Heat Transfer, May 1963.

TABLE I

Single phase flow experiments: argon

ρ_g	Γ_g	Γ_g^i	Γ_g^p	Γ_g^i/Γ_g	Γ_g^p/Γ_g
g/cm^3	g/s	g/s	g/s		
10.0×10^{-3}	234	224	-	0.958	-
16.4 "	226	225	-	0.996	-
22.9 "	221	224	-	1.062	-
27.7 "	217	224	-	1.032	-
36.1 "	158	158	-	1.00	-
" "	464	469	-	1.011	-
" "	467	-	464	-	0.993

Γ_g = Values obtained from orifice readings

Γ_g^i = Values obtained from integration of velocity profiles

Γ_g^p = Values obtained from integration of "Pitot" profile

TABLE II

Two phase flow experiments; round tube 2.5 cm I.D.

MIXTURES	Density	$\bar{G}_g$	$\bar{G}_l$	Γ_g	Γ_l	Γ_g^i	Γ_l^i	Γ_g^i/Γ_g	Γ_l^i/Γ_l
	g/cm^3	g/cm^2s	g/cm^2s	g/s	g/s	g/s	g/s		
Argon-water	$10.0x10^{-3}$	6.7	25.5	33.3	126	24.9	129	0.75	1.025
" "	"	"	135	33.3	667	37	702	1.11	1.036
" "	"	20.1	25.5	99	126	92	133	0.93	1.056
" "	"	"	135	99	667	96	711	0.97	1.066
" "	$36.1x10^{-3}$	24.0	25.5	119	126	120	134	1.01	1.063
" "	"	"	135	119	667	120	685	1.01	1.027
" "	"	73	25.5	357	126	359	134	1.006	1.063
" "	"	"	135	360	667	359	722	0.998	1.066
" "	"	82	206	399	1018	401	1074	1.005	1.055
Argon-Alcohol	$36.1x10^{-3}$	24.0	25.5	119	126	112	139	0.941	1.101
" "	"	"	135	120	667	119	695	0.992	1.042
" "	"	73	25.5	359	126	361	147	1.006	1.165
" "	"	"	135	361	667	359	723	0.997	1.085
" "	$25.4x10^{-3}$	24.0	135	119	667	116	695	0.975	1.042
" "	"	73	135	357	667	357	758	1.00	1.14

$\Gamma_{g,l}$ = Values obtained from orifice readings

$\Gamma^i_{g,l}$ = Values obtained from integration of velocity profiles.

TABLE III

MIXTURES	GEOMETRY: ROUND TUBE	GAS DENSITY g/cm^3	$\bar{G}_g$ g/cm^2s	$\bar{G}_l$ g/cm^2s	$(1-\alpha)^i$	$(1-\bar{\alpha})$	$(1-\alpha)^i/(1-\bar{\alpha})$
Argon-water	2.5 cm I.D.	36.1×10^{-3}	24.0	25.5	0.115	0.115	1.00
"	"	"	"	135	0.277	0.280	0.99
"	"	"	73	25.5	0.0301	0.0375	0.80
"	"	"	"	135	0.102	0.117	0.87
"	"	"	82	206	0.127	0.124	1.02
Argon-ethyl alcohol	"	"	24.0	25.5	0.108	0.115	0.94
"	"	"	"	135	0.280	0.289	0.97
"	"	"	73	25.5	0.0303	0.0183	1.66
"	"	"	"	135	0.098	0.098	1.00

$(1 - \alpha)^i$ = Values obtained from integration of phase distribution profiles

$(1 - \bar{\alpha})$ = Values obtained from direct measurement of the liquid hold-up.

TABLE IV

PHYSICAL PROPERTIES

FLUID	θ °C	P kg/cm^2(a)	ρ g/cm^3	μ poise	γ dyn/cm
Water	18	up to 22	1.00	1.06×10^{-2}(2)	73.0(2)(+)
"	285.5	70	0.742(4)	9.5×10^{-4}(4)	18.2(5)
Ethyl Alcohol(°)	20	up to 22	0.789(6)	1.20×10^{-2}(6)	22.5(6)
Argon	18	21.8	36.1×10^{-3}(1)	2.27×10^{-4}(3)	
"	18	11.5	18.8×10^{-3}(1)	2.25×10^{-4}(3)	
"	18	6.15	10.0×10^{-3}(1)	2.24×10^{-4}	
Steam	285.5	70	35.9×10^{-3}(4)	2.05×10^{-4}	

(+) At atmospheric pressure

(°) Alcohol Aethylicus anhydricus 99.9% by vol. - Carlo Erba - Milano

(1) Tables of thermodynamic and Trasport Properties by S. Hilsenrath et al. Pergamon Press - 1960.

(2) Handbook of Chemistry and Physics - C.D. Hodgman ed. 40th, 1958-59.

(3) Nuclear Enginnering Handbook - H. Etherington Ed. 1st, 1958.

(4) VDI - Wasserdamptafeln by E. Schmidt VDI 6th Edition (Kcal; at;) Springer Verlag, R. Odernburg, 1963.

(5) S.S. Kutateladze - Heat Trasfer in condensation and boiling - AEC-TR 3770 - Appendix I.

(6) International Critical Tables - Mc Graw Hill Book Company - New York 1933.

TABLE V

MIXTURES	Geometry: Round Tube	Gas density	PHASE DISTRIBUTION $\bar{G}_g$	PHASE DISTRIBUTION $\bar{G}_l$	FILM THICKNESS $\bar{G}_g$	FILM THICKNESS $\bar{G}_l$
		g/cm^3	g/cm^2s	g/cm^2s	g/cm^2s	g/cm^2s
Argon-water	2.5 cm I.D.	10.0×10^{-3}	6 ÷ 20	25 ÷ 135	4 ÷ 26	22 ÷ 119
" "	"	36.1×10^{-3}	24 ÷ 82	25 ÷ 206	16 ÷ 200	18 ÷ 206
Argon-alcohol	"	36.1×10^{-3}	24 ÷ 73	25 ÷ 135	-	-
" "	"	25.4×10^{-3}	24 ÷ 73	135	-	-
Argon-water	1.5 cm I.D.	36.1×10^{-3}	-	-	16 ÷ 82	22 ÷ 206

TABLE VI

Argon-water mixture; round tube 2,5 cm I.D. $\rho_g = 36.1 \times 10^{-3}$ g/cm^3

$\bar{G}_g$ g/cm^{2}s	$\bar{G}_l$ g/cm^{2}s	s cm
16.0	18.1	5.6×10^{-2}
"	22.1	6.2 "
"	28.5	7.4 "
"	38.2	9.2 "
"	51	11.0 "
"	66	12.7 "
"	91	15.5 "
"	119	16.5 "
"	157	17.4 "
"	206	18.8 "
21.3	18.1	4.30 "
"	22.1	4.93 "
"	28.5	5.7 "
"	38.2	7.3 "
"	51	9.2 "
"	66	11.3 "
"	91	12.2 "
"	119	13.3 "
"	157	15.0 "
"	206	16.1 "
27.7	18.1	3.43 "
"	22.1	3.94 "
"	28.5	4.76 "
"	38.2	6.1 "
"	51	7.4 "
"	66	8.9 "
27.7	91	10.0×10^{-2}
"	119	10.7 "
"	157	11.7 "
"	206	13.0 "
35.0	18.1	2.76 "
"	22.1	3.21 "
"	28.5	3.77 "
"	38.2	4.67 "
"	51	5.8 "
"	66	7.35 "
"	91	8.0 "
"	119	8.5 "
"	157	9.3 "
"	206	10.7 "
47	18.1	2.14 "
"	22.1	2.45 "
"	28.5	2.96 "
"	38.2	3.72 "
"	51	4.47 "
"	66	5.2 "
"	91	5.9 "
"	119	6.2 "
"	157	6.95 "
"	206	7.7 "
62	22.1	1.88 "
"	38.2	2.55 "
62	51	2.90×10^{-2}
"	66	3.38 "
"	91	3.96 "
"	119	4.35 "
"	157	4.86 "
"	206	5.45 "
82	22.1	1.26 "
"	28.5	1.49 "
"	38.2	1.71 "
"	51	1.91 "
"	66	2.20 "
"	91	2.53 "
"	119	2.93 "
"	157	3.39 "
"	206	3.94 "
95	22.1	0.92 "
"	28.5	1.05 "
"	38.2	1.25 "
"	51	1.51 "
"	66	1.68 "
"	91	1.94 "
"	119	2.24 "
"	157	2.67 "
"	206	3.27 "

TABLE VI (cont.)

$\bar{G}_g$ g/cm^{2}s	$\bar{G}_l$ g/cm^{2}s	s cm
127	22.1	0.56×10^{-2}
"	28.5	0.61 "
"	38.2	0.69 "
"	51	0.78 "
"	66	0.83 "
"	91	1.00 "
"	119	1.12 "
"	157	1.35 "
172	22.1	0.360 "
"	28.5	0.377 "
"	38.2	0.395 "
"	51	0.417 "
"	66	0.450 "
"	91	0.460 "
"	119	0.57 "
"	157	0.66 "
200	22.1	0.286 "
"	28.5	0.309 "
"	38.2	0.314 "
"	51	0.325 "
"	66	0.343 "

TABLE VII

Argon-water mixture; round tube 2.5 cm I.D.

$\rho_g = 10.0 \times 10^{-3}$ g/cm^3

$\bar{G}_g$	$\bar{G}_l$	s
g/cm^{2}s	g/cm^{2}s	cm
4.52	22.1	8.9×10^{-2}
"	38.2	11.6 "
"	66	14.7 "
"	91	17.5 "
"	119	18.6 "
7.6	22.1	5.8 "
"	38.2	8.2 "
"	66	10.8 "
"	91	12.4 "
"	119	13.0 "
12.9	22.1	3.70 "
"	38.2	5.3 "
"	66	6.8 "
"	91	8.1 "
"	119	8.4 "
22.6	22.1	2.28 "
"	38.2	3.37 "
"	66	4.48 "
"	91	4.66 "
"	119	5.0 "
26.3	22.1	1.89 "
"	38.2	2.74 "
"	66	3.78 "
"	91	4.12 "
"	119	4.54 "

TABLE VIII

Argon-water mixture; round tube 1.5 cm I.D.

$$\rho_g = 36.1 \times 10^{-3} \text{ g/cm}^3$$

$\bar{G}_g$	$\bar{G}_l$	s
g/cm^2s	g/cm^2s	cm
16.0	22.1	3.78×10^{-2}
"	38.2	5.6 "
"	91	9.2 "
"	206	12.4 "
27.8	22.1	2.57 "
"	38.2	3.79 "
"	91	6.6 "
"	206	8.1 "
47	22.1	1.63 "
"	38.2	2.47 "
"	91	4.22 "
"	206	5.0 "
82	22.1	0.87 "
"	38.2	1.23 "
"	91	1.88 "
"	206	2.63 "

TABLE IX

Argon-water mixture; round tube 2.5 cm I.D.

$\bar{G}_g$ = 24.0 g/cm^{2}s; $\bar{G}_l$ = 25.5 g/cm^{2}s

$\rho_g = 36.1 \times 10^{-3}$ g/cm^3

y cm	ΔP_p dyn/cm^2	G_g g/cm^{2}s	G_l g/cm^{2}s	1-α	S
1.250	2.05×10^4	34.7	3.2	0.00285	0.84
0.871	1.84 "	33.2	3.42	0.00382	1.03
0.629	1.57 "	29.8	4.28	0.0053	1.03
0.376	1.25 "	23.0	9.3	0.0164	1.15
0.214	1.21 "	16.5	23.4	0.063	1.32
0.120+	-	11.3	57	0.157	-
0.0695+	-	6.2	94	0.355	-
0.0395+	-	2.74	128	0.62	-
0.0250+	-	0.96	130	0.83	-
0.0165+	-	0.42	117	0.91	-
0.0065+	-	0.068	61	0.97	-

Note: the points signed with + in the "y" column were obtained with "the film sampling probe"(4). The corresponding 1-α values were derived with the assumption S = 1.

Integral values obtained with "the film sampling probe":

y' cm	Γ_l g/s	Γ_g g/s
0.013	6.1	0.0068
0.020	12.5	0.029
0.030	22.5	0.103
0.049	40.8	0.50
0.090	70	2.40
0.150	93	7.3

TABLE X

Argon-water mixtures; round tube 2.5 cm I.D.

$\bar{G}_g$ = 24.0 g/cm^{2}s ; $\bar{G}_l$ = 135 g/cm^{2}s

ρ_g = 36.1x10^{-3} g/cm^3

y cm	ΔP_p dyn/cm^2	G_g g/cm^{2}s	G_l g/cm^{2}s	1-α	S
1.250	1.14x10^5	44.6	79	0.069	1.15
0.871	1.12 "	40.6	89	0.078	1.07
0.629	1.03 "	35.6	95	0.101	1.16
0.376	0.93 "	25.2	137	0.201	1.27
0.214	0.77 "	15.8	182	0.367	1.40
0.1375$^+$	-	8.1	189	0.459	-
0.1025$^+$	-	6.7	211	0.53	-
0.0650$^+$	-	5.2	191	0.57	-
0.0375$^+$	-	3.30	194	0.68	-
0.0190$^+$	-	1.68	197	0.80	-
0.0065$^+$	-	0.73	125	0.98	-

Note: the points signed with + in the "y" column were obtained with "the film sampling probe"[4]. The corresponding 1-α values were derived with the assumption S = 1.

Integral values obtained with "the film sampling probe"

y'	Γ_l	Γ_g
cm	g/s	g/s
0.013	12.6	0.0074
0.025	30.8	0.163
0.050	68	0.79
0.080	111	1.97
0.125	178	4.15
0.150	211	5.6

TABLE XI

Argon-water mixture; round tube 2.5 cm I.D.

$\bar{G}_g = 73$ g/cm^{2}s; $\bar{G}_l = 25.5$ g/cm^{2}s

$\rho_g = 36.1 \times 10^{-3}$ g/cm^3

y cm	ΔP_p dyn/cm^2	G_g g/cm^{2}s	G_l g/cm^{2}s	1-α	S
1.250	1.57×10^5	99	13.7	0.0078	1.57
0.871	1.50 "	94	14.5	0.0075	1.35
0.629	1.34 "	86	15.3	0.0070	1.10
0.376	1.12 "	76	17.6	0.0092	1.10
0.214	0.93 "	64	18.2	0.0094	0.93
0.125+	-	62	25.3	0.0145	-
0.0750+	-	54	36.5	0.0237	-
0.0375+	-	35.5	78	0.073	-
0.0210+	-	20.8	147	0.203	-
0.0150+	-	14.1	230	0.370	-
0.0065+	-	2.25	196	0.76	-

Note: the points signed with + in the "y" column were obtained with "the film sampling probe"[4]. The corresponding 1-α values were derived with the assumption S = 1.

Integral values obtained with "film sampling probe"

y'	Γ_l	Γ_g
cm	g/s	g/s
0.013	19.8	0.231
0.017	26.9	0.67
0.025	35.9	1.95
0.050	50	8.7
0.100	63	28.9
0.150	71	51

TABLE XII

Argon-water mixture; round tube 2.5 cm I.D.

$\bar{G}_g = 73$ g/cm^{2}s ; $\bar{G}_l = 135$ g/cm^{2}s

$\rho_g = 36.1 \times 10^{-3}$ g/cm^3

y cm	ΔP_p dyn/cm^2	G_g g/cm^{2}s	G_l g/cm^{2}s	1-α	S
1.250	4.31×10^5	107	100	0.0360	1.12
0.871	4.31 "	101	110	0.0411	1.09
0.629	4.11 "	91	125	0.052	1.10
0.376	4.07 "	80	144	0.063	1.04
0.214	2.80 "	62	129	0.071	1.02
0.125+	-	50	146	0.094	-
0.075+	-	42.9	190	0.138	-
0.044+	-	19.7	255	0.316	-
0.029+	-	13.1	305	0.463	-
0.0165+	-	4.33	325	0.73	-
0.0065+	-	0.48	275	0.95	-

Note: the points signed with + in the "y" column were obtained with "the film sampling probe"[4]. The corresponding 1-α values were derived with the assumption S = 1.

Integral values obtained with "film sampling probe"

y'	Γ_l	Γ_g
cm	g/s	g/s
0.013	27.7	0.049
0.020	45.5	0.283
0.038	87	2.09
0.050	111	3.89
0.100	180	17.9
0.150	229	35.5

TABLE XIII

Argon-water mixtures ; round tube 2.5 cm I.D.

$\bar{G}_g$ = 82 g/cm^{2}s ; $\bar{G}_l$ = 206 g/cm^{2}s

ρ_g = 36.1x10^{-3} g/cm^3

y	ΔP_p	G_g	G_l	1-α	S
cm	dyn/cm^2	g/cm^{2}s	g/cm^2		
1.250	6.91x10^5	126	150	0.0474	1.16
0.871	7.0 "	117	171	0.056	1.11
0.629	7.4 "	106	210	0.073	1.11
0.376	7.0 "	91	240	0.094	1.080
0.214	5.1 "	72	215	0.099	1.019
0.150	3.78 "	61	196	0.111	1.083
0.115$^+$	-	60	213	0.114	-
0.060$^+$	-	36	242	0.197	-
0.035$^+$	-	19.5	316	0.369	-
0.025$^+$	-	15.2	332	0.441	-
0.0165$^+$	-	8.6	376	0.61	-
0.0065$^+$	-	1.53	312	0.88	-

Note: the points signed with + in the "y" column were obtained with "the film sampling probe"[4]. The corresponding 1-α values were derived with the assumption S = 1.

Integral values obtained with "film sampling probe"

y'	Γ_l	Γ_g
cm	g/s	g/s
0.013	31.4	0.154
0.020	52	0.63
0.030	77	1.79
0.040	101	3.28
0.080	173	14.0
0.150	277	46.7

TABLE XIV

Argon-water mixture; round tube 2.5 cm I.D.

$\bar{G}_g = 145.5$ g/cm^{2}s ; $\bar{G}_l = 4.5$ g/cm^{2}s

$\rho_g = 36.1 \times 10^{-3}$ g/cm^3

y cm	G_g g/cm^{2}s	G_l g/cm^{2}s
1.250	184	4.03
0.871	175	3.41
0.629	166	3.50
0.376	152	3.54
0.214	144	3.40
0.073$^+$	-	6.3
0.038$^+$	111	6.0
0.0205$^+$	94	6.7
0.0065$^+$	43.3	75

Note: the points signed with + in the "y" column were been obtained with the "film sampling probe"[4].

Integral values obtained with "the film sampling probe"

y' cm	Γ_l g/s	Γ_g g/s
0.013	0.81	0.455
0.028	0.88	1.55
0.048	0.98	3.20
0.098	1.23	-

TABLE XV

Argon-water mixture; round tube 2.5 cm I.D.

$\bar{G}_g$ = 6.7 g/cm^{2}s; $\bar{G}_l$ = 25.5 g/cm^{2}s

$\rho_g = 10.0 \times 10^{-3}$ g/cm^3

y cm	ΔP_p dyn/cm^2	G_g g/cm^{2}s	G_l g/cm^{2}s	1-α	S
1.250	5.5×10^3	10.4	2.11	0.059	9.8
0.871	4.65 "	9.4	2.56	0.0290	8.5
0.629	4.07 "	8.0	3.99	0.0180	6.1
0.376	4.41 "	5.8	12.9	0.060	2.85
0.214	6.3 "	3.24	31.4	0.156	1.91
0.125$^+$	-	2.04	58	0.221	-
0.085$^+$	-	1.62	75	0.423	-
0.050$^+$	-	0.44	92	0.68	-
0.0215$^+$	-	0.0212	104	0.96	-
0.0065$^+$	-	0.0077	37.5	0.99	-

Note: the points signed with + in the "y" column were obtained with "the film sampling probe"(4). The corresponding 1-α values were derived with the assumption S = 1.

Integral values obtained with "the film sampling probe"

y'	Γ_l	Γ_g
cm	g/s	g/s
0.013	3.78	0.00078
0.030	17.4	0.0049
0.070	45.1	0.137
0.100	61	0.364
0.150	81	1.10

TABLE XVI

Argon-water mixture; round tube 2.5 cm I.D.

$\bar{G}_g = 6.7$ g/cm^{2}s; $\bar{G}_l = 135$ g/cm^{2}s

$\rho_g = 10.0 \times 10^{-3}$ g/cm^3

y cm	ΔP_p dyn/cm^2	G_g g/cm^{2}s	G_l g/cm^{2}s	1-α	S
1.250	0.73×10^5	14.9	51	0.0419	1.26
0.871	0.88 "	14.1	68	0.057	1.27
0.629	0.97 "	11.6	96	0.097	1.30
0.376	1.09 "	9.5	156	0.206	1.38
0.214	0.86 "	4.07	196	0.367	1.21
0.1675+	-	2.99	210	0.387	-
0.123+	-	2.14	207	0.492	-
0.075+	-	1.60	199	0.55	-
0.0375+	-	0.58	192	0.71	-
0.0190+	-	0.33	185	0.85	-
0.0065+	-	0.062	117	0.95	-

Note: the points signed with + in the "y" column were obtained with "the film sampling probe"(4). The corresponding 1-α values were derived with the assumption S = 1.

Integral values obtained with "the film sampling probe"

y'	Γ_l	Γ_g
cm	g/s	g/s
0.013	11.8	0.0063
0.025	28.8	0.0364
0.050	65.4	0.148
0.100	138	0.74
0.146	206	1.45
0.189	268	2.35

TABLE XVII

Argon-water mixture; round tube 2.5 cm I.D.

$\bar{G}_g$ = 20.1 g/cm^{2}s; $\bar{G}_l$ = 25.5 g/cm^{2}s

$\rho_g = 10.0 \times 10^{-3}$ g/cm^3

y cm	ΔP_p dyn/cm^2	G_g g/sm^{2}s	G_l g/cm^{2}s	1-α	S
1.250	6.51×10^4	29.8	8.3	0.00333	1.19
0.871	6.0 "	27.8	8.7	0.00355	1.14
0.629	5.1 "	24.9	8.3	0.00342	1.03
0.376	3.78 "	20.2	9.3	0.00498	1.08
0.214	2.86 "	15.6	12.8	0.0099	1.22
0.125$^+$	-	13.0	32.0	0.0240	-
0.075$^+$	-	7.7	72	0.0853	-
0.037$^+$	-	3.12	152	0.327	-
0.021$^+$	-	1.41	187	0.54	-
0.0155$^+$	-	1.00	194	0.65	-
0.0065	-	0.208	127	0.82	-

Note: the points signed with + in the "y" column were obtained with "the film sampling probe"(4). The corresponding 1- α values were derived with the assumption S = 1.

Integral values obtained with the "film sampling probe"

y' cm	Γ_l g/s	Γ_g g/s
0.013	12.8	0.0209
0.018	20.4	0.060
0.024	29.0	0.125
0.050	59	0.74
0.100	85	3.61
0.150	94	8.3

TABLE XVIII

Argon-water mixture; round tube 2.5 cm I.D.

$\bar{G}_g = 20.1$ g/cm^{2}s; $\bar{G}_l = 135$ g/cm^{2}s

$\rho_g = 10.0 \times 10^{-3}$ g/cm^3

y	ΔP_p	G_g	G_l	1-α	S
cm	dy/cm^2	g/cm^{2}s	g/cm^{2}s		
1.250	1.87×10^5	33.4	46.8	0.0165	1.20
0.871	2.10 "	30.9	60	0.0272	1.43
0.629	2.50 "	26.7	93	0.0400	1.19
0.376	3.01 "	22.4	137	0.0682	1.14
0.214	2.42 "	17.1	161	0.109	1.29
0.080+	-	6.3	253	0.288	-
0.045+	-	3.67	298	0.448	-
0.0215+	-	1.12	291	0.72	-
0.0065+	-	0.261	236	0.91	-

Note: the points signed with + in the column "y" were obtained with "the film sampling probe"[4]. The corresponding 1-α values were derived with the assumption S = 1.

Integral values obtained with "the film sampling probe"

y'	Γ_l	Γ_g
cm	g/s	g/s
0.013	23.8	0.0264
0.030	62	0.173
0.060	129	1.01
0.100	203	2.87

TABLE XIX

Argon-water mixture; round tube 2.5 cm I.D.

$\bar{G}_g = 22.6$ g/cm^{2}s; $\bar{G}_l = 91$ g/cm^{2}s

$\rho_g = 10.0 \times 10^{-3}$ g/cm^3

y cm	ΔP_p dyn/cm^2	G_g g/cm^{2}s	G_l g/cm^{2}s	1-α	S
1.250	1.77×10^5	34.9	32.4	0.0090	0.98
0.871	1.75 "	33.5	38.0	0.0121	1.08
0.629	1.69 "	29.2	48.1	0.0182	1.12
0.376	1.91 "	23.9	76	0.0352	1.14
0.214	1.69 "	17.8	104	0.066	1.22

TABLE XX

Argon-alcohol mixture; round tube 2.5 cm I.D.

$\bar{G}_g$ = 24.0 g/cm^{2}s; $\bar{G}_l$ = 135 g/cm^{2}s

$\rho_g = 25.4 \times 10^{-3}$ g/cm^3

y	ΔP_p	G_g	G_l	$1-\alpha$	S
cm	dyn/cm^2	g/cm^2	g/cm^{2}s		
1.250	16.8×10^4	37.9	97	0.082	1.08
0.871	18.3 "	35.2	113	0.096	1.03
0.629	19.3 "	31.3	136	0.128	1.05
0.376	18.0 "	25.8	156	0.168	1.04
0.214	12.7 "	20.6	143	0.196	1.09
0.150	9.7 "	16.7	149	0.266	1.26
0.135+	-	14.7	149	0.247	-
0.100+	-	11.4	156	0.307	-
0.0650+	-	7.2	157	0.411	-
0.0400+	-	4.3	171	0.56	-
0.0240+	-	1.7	169	0.77	-
0.0155+	-	0.89	186	0.87	-
0.0065+	-	0.137	103	0.96	-

Note: the points signed with + in the "y" column were been obtained with the "film sampling probe"(4). The corresponding $1-\alpha$ values were derived with the assumption S = 1.

Integral values obtained with "the film sampling probe"

y'	Γ_l	Γ_g
cm	g/s	g/s
0.013	1.08	-
0.018	1.82	-
0.030	3.45	1.99×10^{-2}
0.050	6.2	9.0 "
0.080	9.9	26.4 "
0.120	15.0	63 "
0.150	18.6	98 "

TABLE XXI

Argon-alcohol mixture; round tube 2.5 cm I.D.

$\bar{G}_g = 73$ g/cm^{2}s; $\bar{G}_l = 135$ g/cm^{2}s

$\rho_g = 25.4 \times 10^{-3}$ g/cm^3

y	ΔP_p	G_g	G_l	1-α	S
cm	dyn/cm^2	g/cm^{2}s	g/cm^{2}s		
1.250	56×10^4	87	127	0.049	1.09
0.871	55 "	85	125	0.048	1.07
0.629	60 "	81	156	0.064	1.11
0.376	59 "	77	159	0.066	1.06
0.214	60 "	68	194	0.089	1.07
0.150	54 "	65	178	0.084	1.03
0.095+	-	65	171	0.079	-
0.065+	-	61	129	0.063	-
0.0400+	-	60	87	0.044	-
0.0240+	-	52	46	0.0280	-
0.0155+	-	43.2	28.3	0.0206	-
0.0065+	-	34.7	18.2	0.0166	-

Note: the points signed with + in the "y" column were been obtained with the "film sampling probe"(4). The corresponding 1-α values were been derived with the assumption S = 1.

Integral values obtained with the "film sampling probe"

y'	Γ_l	Γ_g
cm	g/s	g/s
0.013	0.190	0.361
0.018	0.303	0.53
0.030	0.74	1.03
0.050	2.13	1.99
0.080	5.2	3.47
0.110	9.3	5.0

TABLE XXII

Argon-alcohol mixture; round tube 2.5 cm I.D.

$\bar{G}_g = 24.0$ g/cm^{2}s; $\bar{G}_l = 25.5$ g/cm^{2}s

$\rho_g = 36.1 \times 10^{-3}$ g/cm^3

y cm	ΔP_p dyn/cm^2	G_g g/cm^{2}s	G_l g/cm^{2}s	1-α	S
1.250	3.27×10^4	35.8	16.7	0.0232	1.11
0.871	3.18 "	32.5	19.8	0.0286	1.06
0.629	2.96 "	30.1	20.5	0.0306	1.01
0.376	2.60 "	24.7	25.6	0.0462	1.02
0.214	1.98 "	20.7	25.1	0.056	1.06
0.150	1.63 "	17.4	28.4	0.081	1.17
0.135+	-	16.3	32.1	0.083	-
0.100+	-	13.6	40.6	0.120	-
0.065+	-	8.1	50	0.220	-
0.040+	-	4.55	68	0.404	-
0.0240+	-	0.40	75	0.89	-
0.0155+	-	0.108	75	0.97	-
0.0065+	-	0.0138	29.9	0.99	-

Note: the points signed with + in the "y" column were obtained with "the film sampling probe"[4]. The corresponding 1-α values were derived with the assumption S = 1.

Integral values obtained with "the film sampling probe"

y'	Γ_l	Γ_g
cm	g/s	g/s
0.013	3.02	0.00144
0.018	5.9	0.0056
0.030	12.8	0.0425
0.050	23.2	0.74
0.080	34.2	2.56
0.120	45.7	6.5
0.150	57	10.0

TABLE XXIII

Argon-alcohol mixture; round tube 2.5 cm I.D.

$\bar{G}_g$ = 24.0 g/cm^{2}s; $\bar{G}_l$ = 135 g/cm^{2}s

$\rho_g = 36.1 \times 10^{-3}$ g/cm^3

y	ΔP_p	G_g	G_l	1-α	S
cm	dyn/cm^2	g/cm^{2}s	g/cm^{2}s		
1.250	1.39×10^5	40.1	112	0.128	1.15
0.871	1.47 "	36.4	129	0.152	1.10
0.629	1.45 "	33.2	146	0.188	1.15
0.376	1.23 "	26.4	154	0.234	1.15
0.214	0.85 "	21.0	133	0.250	1.15
0.135$^+$	-	14.7	143	0.308	-
0.100$^+$	-	11.9	145	0.357	-
0.065$^+$	-	7.5	139	0.476	-
0.040$^+$	-	4.24	152	0.60	-
0.024$^+$	-	1.47	160	0.82	-
0.0155$^+$	-	0.92	148	0.88	-
0.0065$^+$	-	0.163	85	0.96	-

Note: the points signed with + in the "y" column were obtained with "the film sampling probe"(4). The corresponding 1-α values were derived with the assumption S = 1.

Integral values obtained with "the film sampling probe"

y'	Γ_l	Γ_g
cm	g/s	g/s
0.013	8.5	0.0165
0.018	14.3	0.052
0.030	29.0	0.188
0.050	52	0.83
0.080	83	2.52
0.120	125	6.0
0.150	155	9.1

TABLE XXIV

Argon-alcohol mixture; round tube 2.5 I.D.

$\bar{G}_g$ = 73 g/cm^{2}s $\bar{G}_l$ = 25.5 g/cm^{2}s

ρ_g = 36.1x10^{-3} g/cm^3

y	ΔP_p	G_l	G_g	1-α	S
cm	dyn/cm^2	g/cm^{2}s	g/cm^{2}s		
1.250	1.47x10^5	25.5	86	0.0185	1.39
0.871	1.42 "	26.9	84	0.0203	1.42
0.629	1.36 "	27.3	81	0.0209	1.40
0.376	1.30 "	33.5	74	0.0254	1.25
0.214	1.19 "	32.5	70	0.0258	1.24
0.135$^+$	-	28.7	65	0.0197	-
0.100$^+$	-	34.5	74	0.0209	-
0.065$^+$	-	36.2	59	0.0272	-
0.040$^+$	-	24.6	60	0.0183	-
0.024$^+$	-	16.0	54	0.0133	-
0.0155$^+$	-	11.4	44.2	0.0117	-
0.0065$^+$	-	9.0	34.0	0.0120	-

Note: the points signed with + in the "y" column were obtained with "the film sampling probe"[4]. The corresponding 1-α values were derived with the assumption S = 1.

Integral values obtained with "the film sampling probe"

y'	Γ_l	Γ_g
cm	g/s	g/s
0.013	0.91	3.42
0.018	1.35	5.1
0.030	2.82	10.1
0.050	6.6	19.3
0.080	14.7	32.5
0.120	24.7	54
0.151	30.9	68

TABLE XXV

Argon-alcohol mixture; round tube 2.5 cm I.D.

$\bar{G}_g$ = 73 g/cm^{2}s; $\bar{G}_l$ = 135 g/cm^{2}s

$\rho_g = 36.1 \times 10^{-3}$ g/cm^3

y	ΔP_p	G_g	G_l	$1-\alpha$	S
cm	dyn/cm^2	g/cm^{2}s	g/cm^{2}s		
1.250	4.44×10^5	94	129	0.064	1.09
0.871	4.44 "	93	134	0.068	1.09
0.629	4.40 "	84	148	0.078	1.05
0.376	4.36 "	79	167	0.096	1.09
0.214	4.12 "	67	183	0.115	1.04
0.150	3.47 "	63	161	0.112	1.08
0.135$^+$	-	61	162	0.109	-
0.100$^+$	-	64	143	0.092	-
0.065$^+$	-	50	99	0.083	-
0.040$^+$	-	49	73	0.064	-
0.024$^+$	-	31.2	59	0.080	-
0.0155$^+$	-	24.4	90	0.144	-
0.0065$^+$	-	5.4	96	0.45	-

Note: the points signed with + in the "y" column were obtained with "the film sampling probe"[4]. The corresponding $1-\alpha$ values were derived with the assumption S = 1.

Integral values obtained with "the film sampling probe"

y'	Γ_l	Γ_g
cm	g/s	g/s
0.013	9.7	0.55
0.018	13.1	1.49
0.030	18.6	4.38
0.050	29.1	11.8
0.080	51	23.0
0.120	93	41.6
0.150	127	54

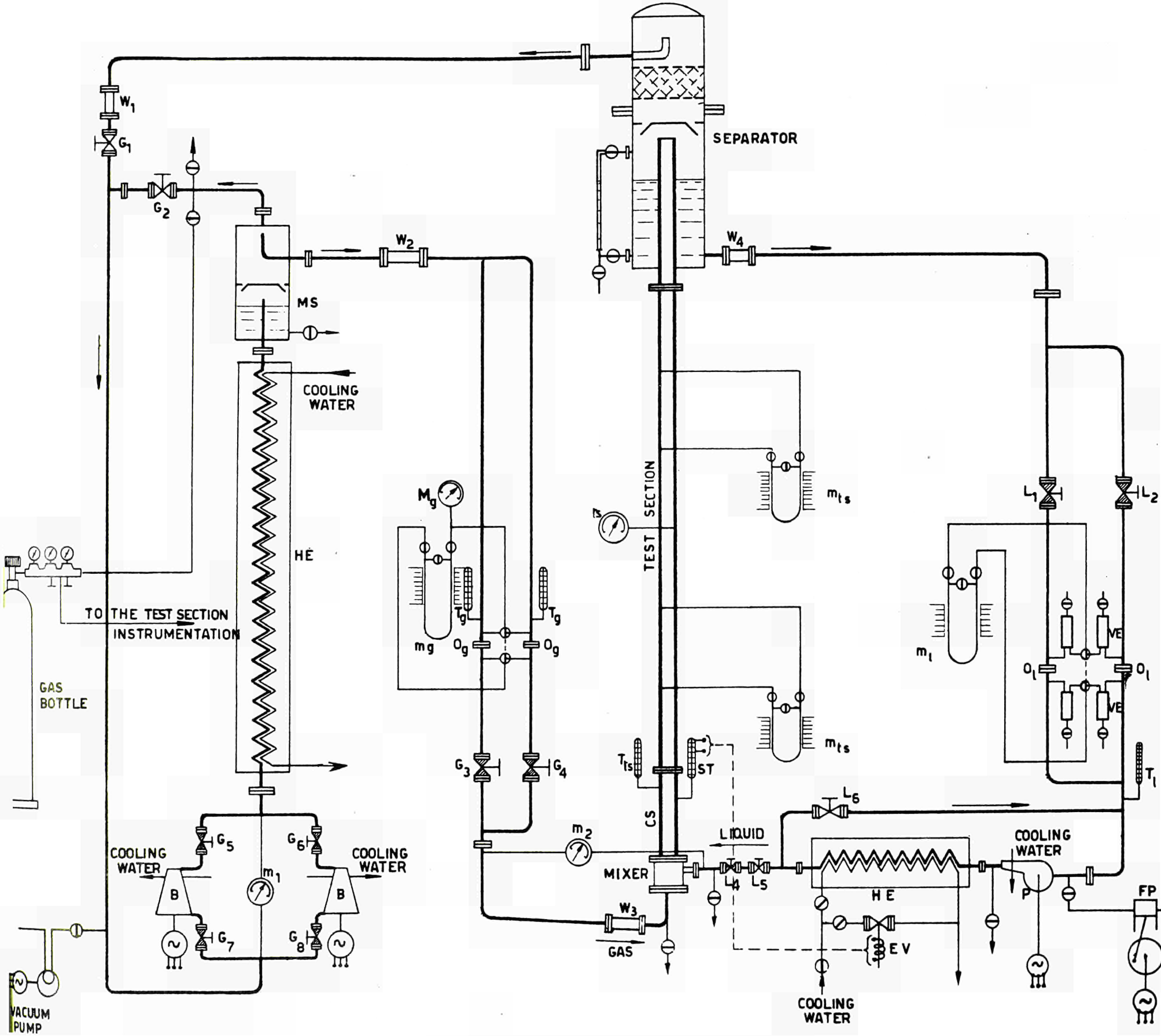

⋈	stop valve
⋈	control valve
B	blower
CS	calming section
EV	electromagnetic valve
FP	liquid feeding pump
G	gas line valve
HE	heat exchanger
L	liquid line valve
m	differential manometer
M	manometer
MS	moisture separator
O	orifice
P	pump
ST	switch thermometer
T	thermometer
VE	vent
W	transparent window

Subscripts

g	gas
ts	test section
l	liquid

Fig. 1 - Schematic flow sheet of the circuit.

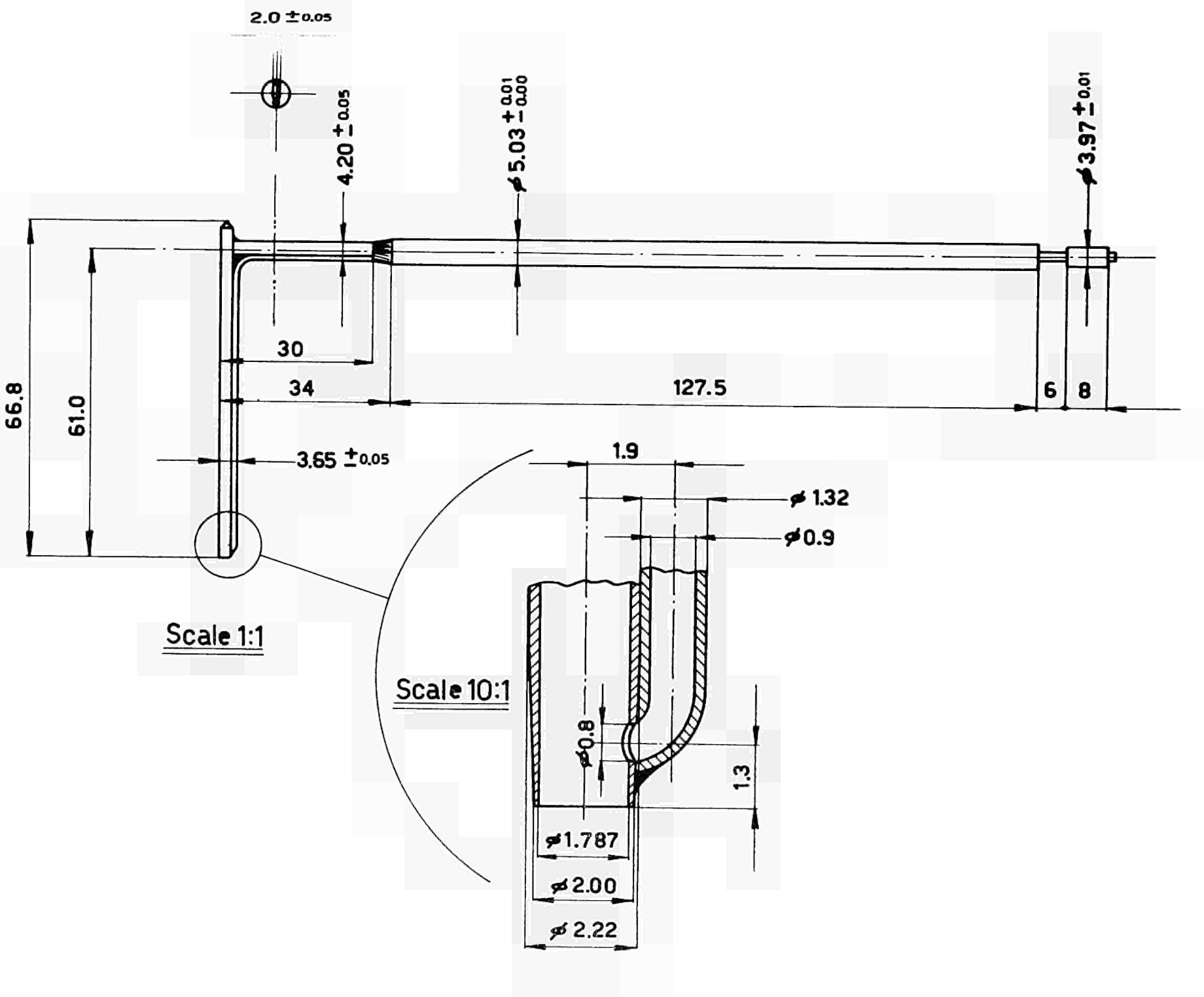

Fig. 2 - Main dimension of the sampling probe.

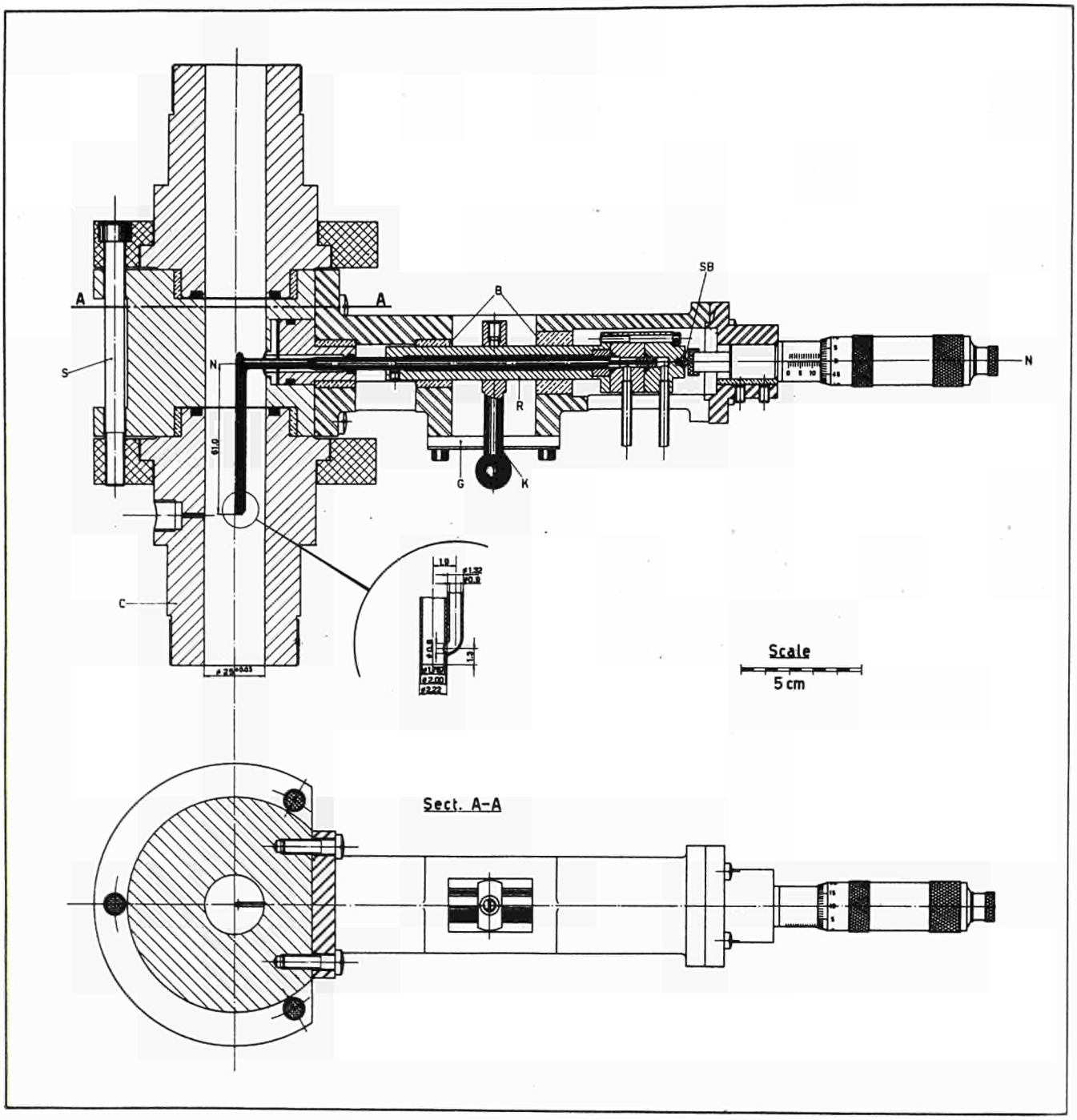

Fig. 3 - The device for the introduction and positioning of the sampling probe.

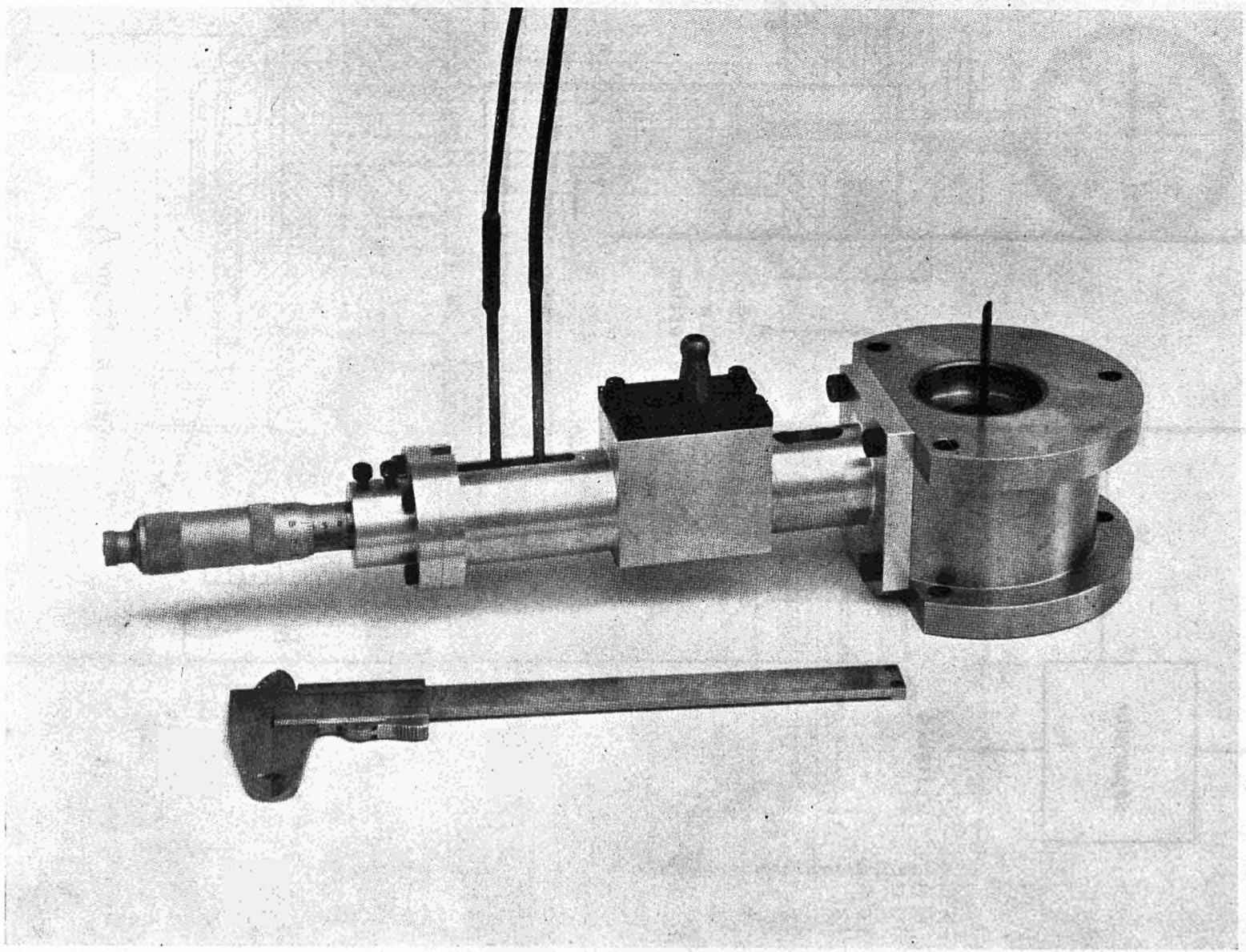

Fig. 4 - The sampling probe apparatus.

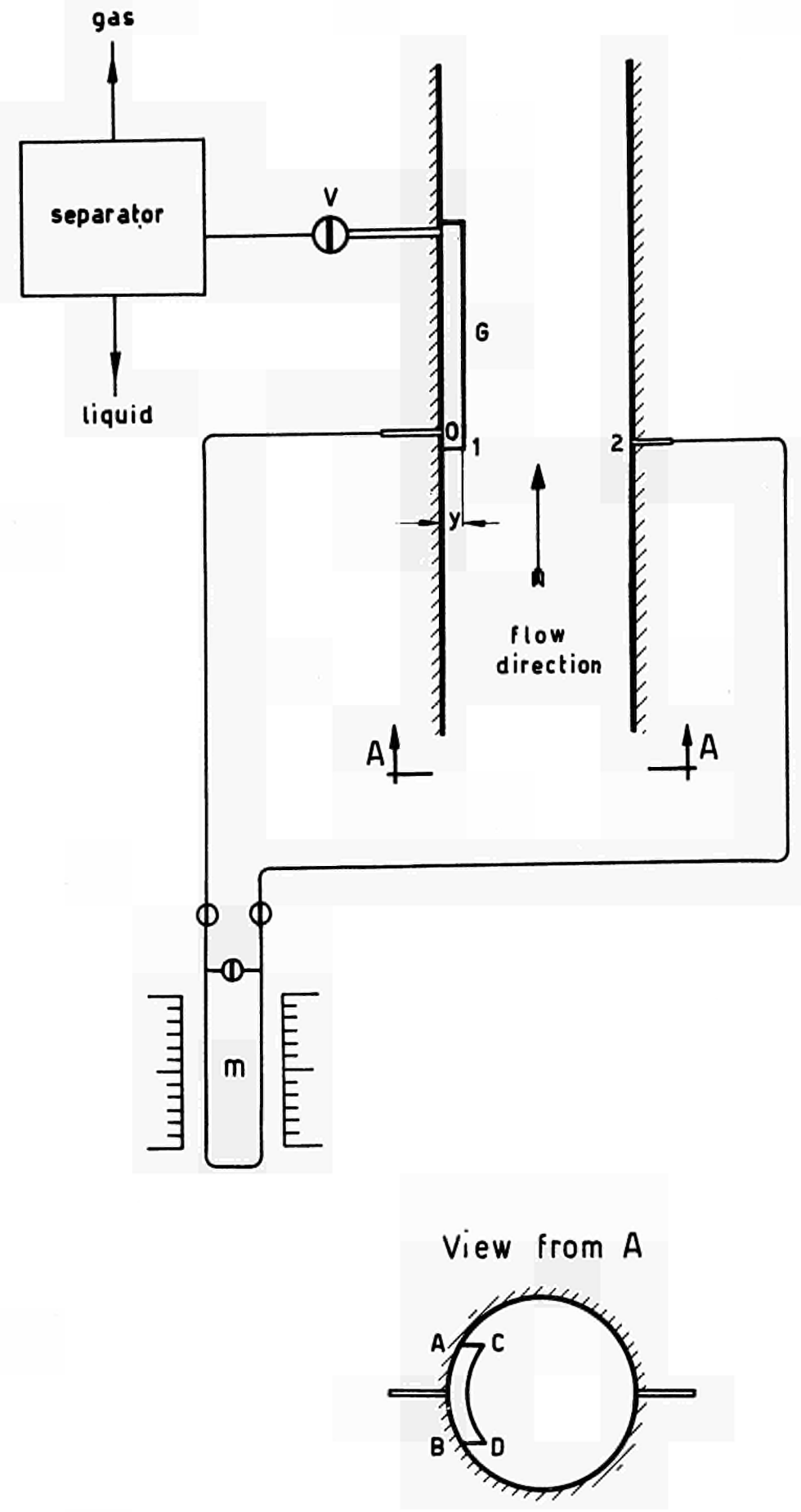

Fig. 5 - The basic "film" sampling probe circuit.

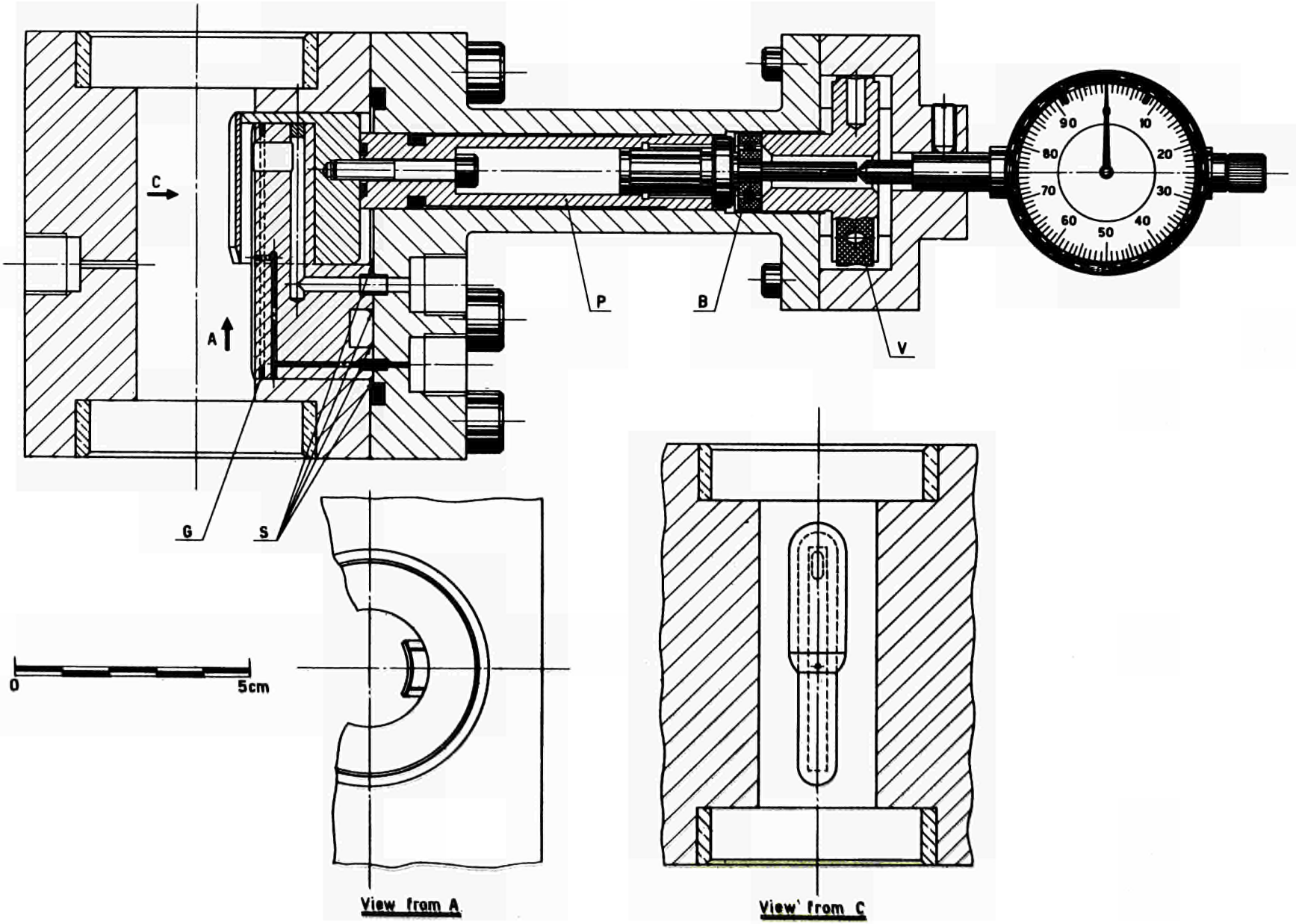

Fig. 6 - The device for the introduction and positioning of the "film" sampling probe.

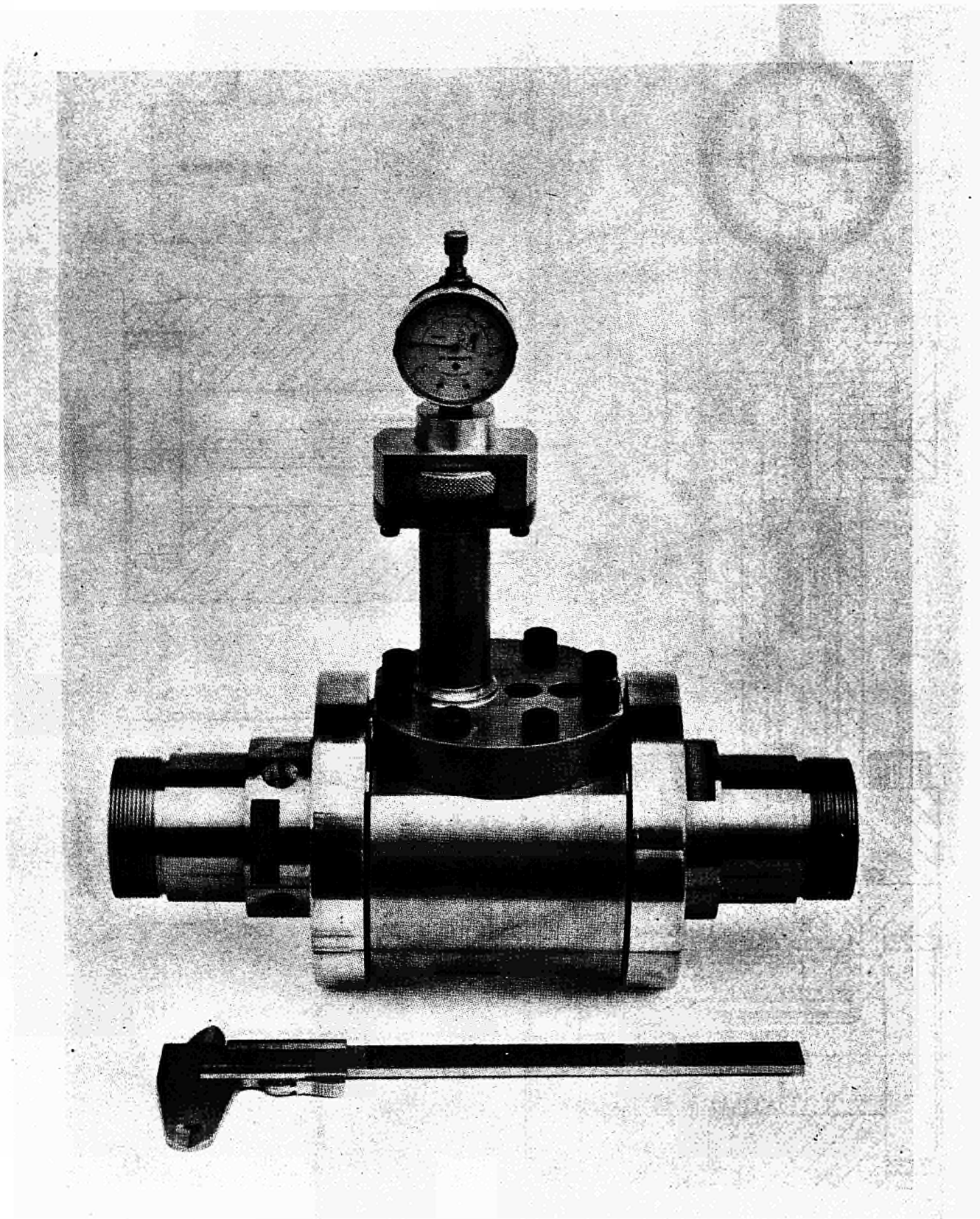

Fig. 7 - The "film" sampling probe apparatus.

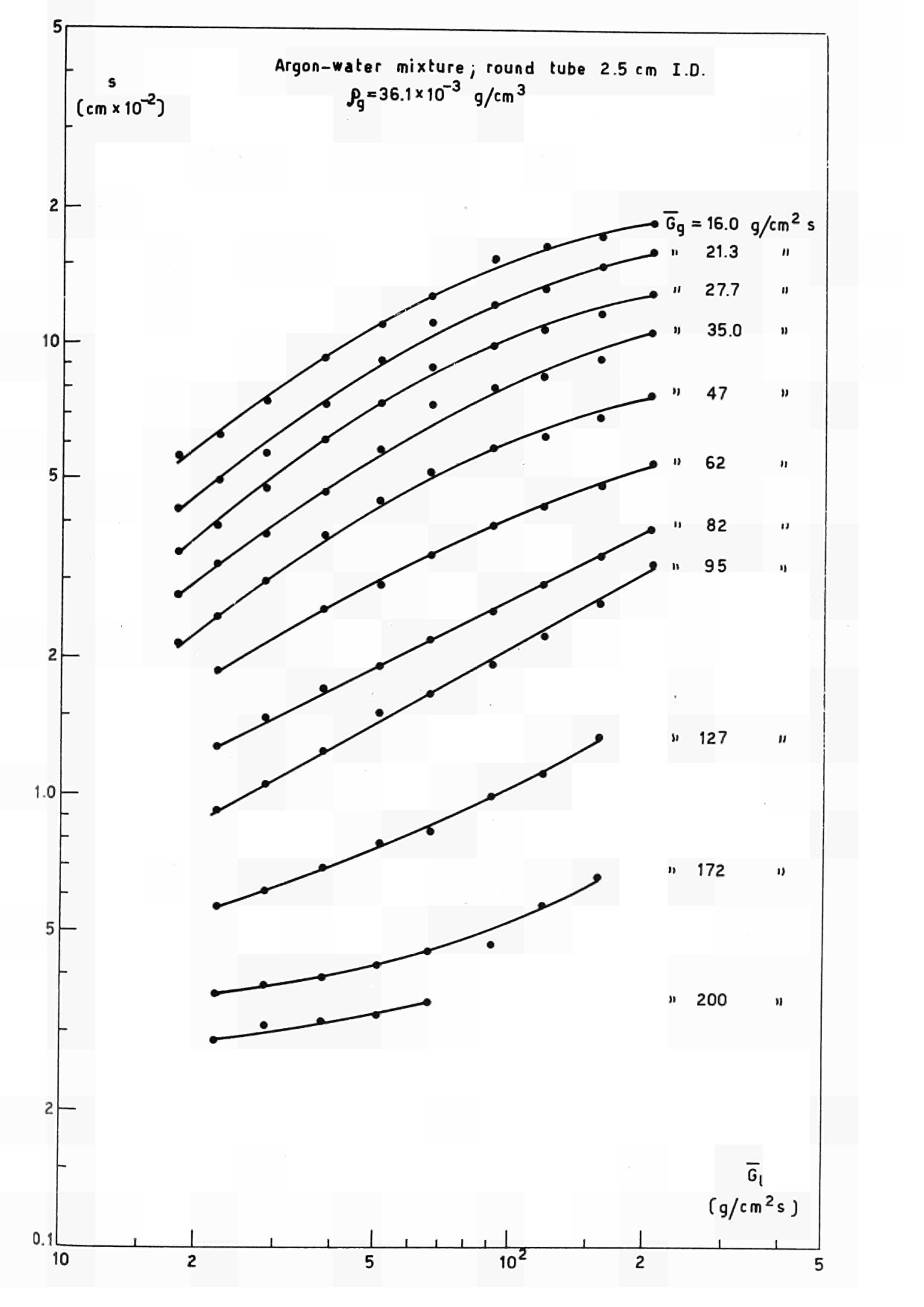
Argon–water mixture ; round tube 2.5 cm I.D.
$\rho_g = 36.1 \times 10^{-3}$ g/cm^3
s
(cm x 10^{-2})
$\overline{G}_g$ = 16.0 g/cm^2 s
" 21.3 "
" 27.7 "
" 35.0 "
" 47 "
" 62 "
" 82 "
" 95 "
" 127 "
" 172 "
" 200 "
$\overline{G}_l$
(g/cm^{2}s)
5
2
10
5
2
1.0
5
2
0.1
10
2
5
10^2
2
5

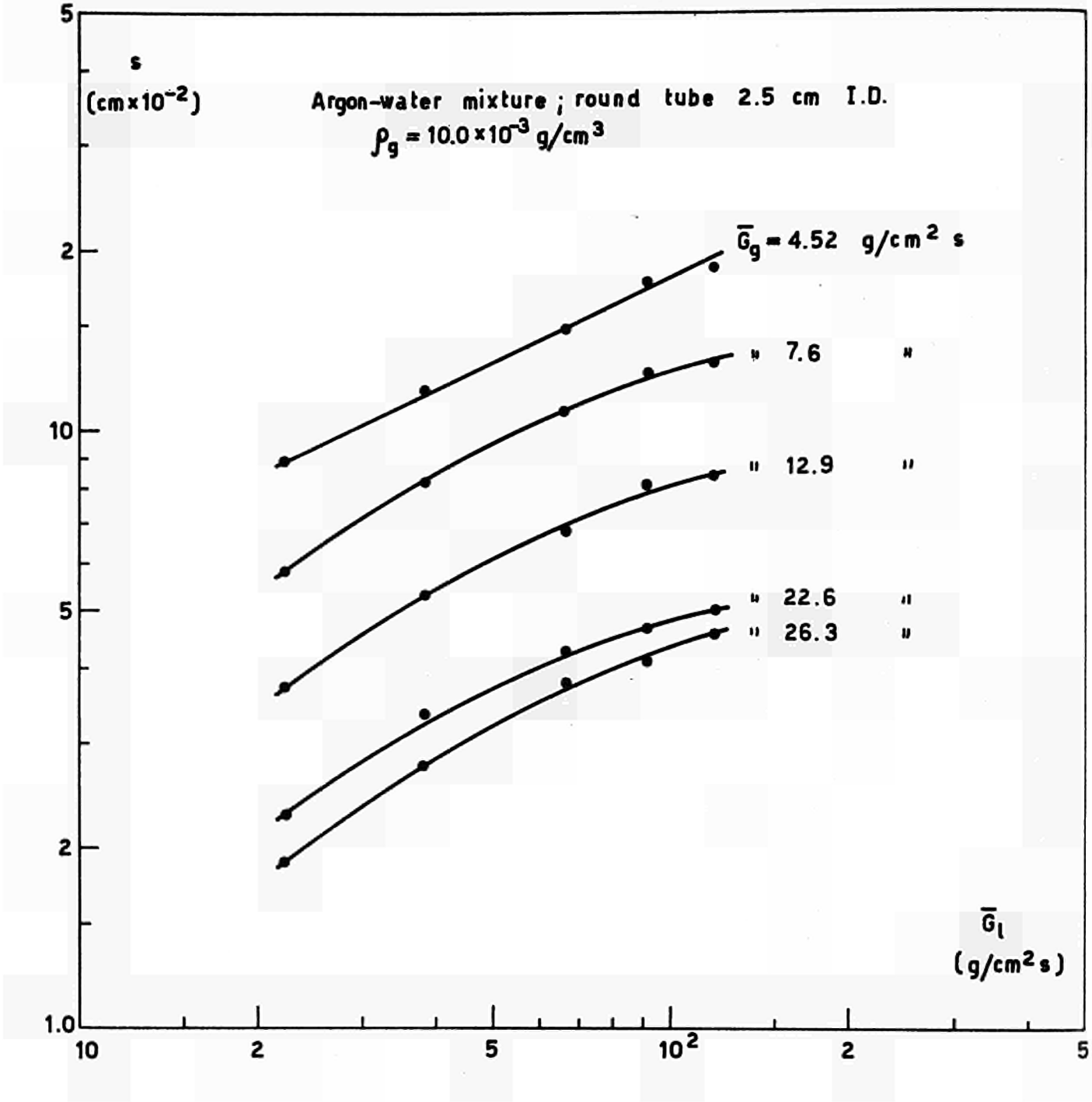

Fig. 9 - Film thickness vs. average specific mass flowrate.

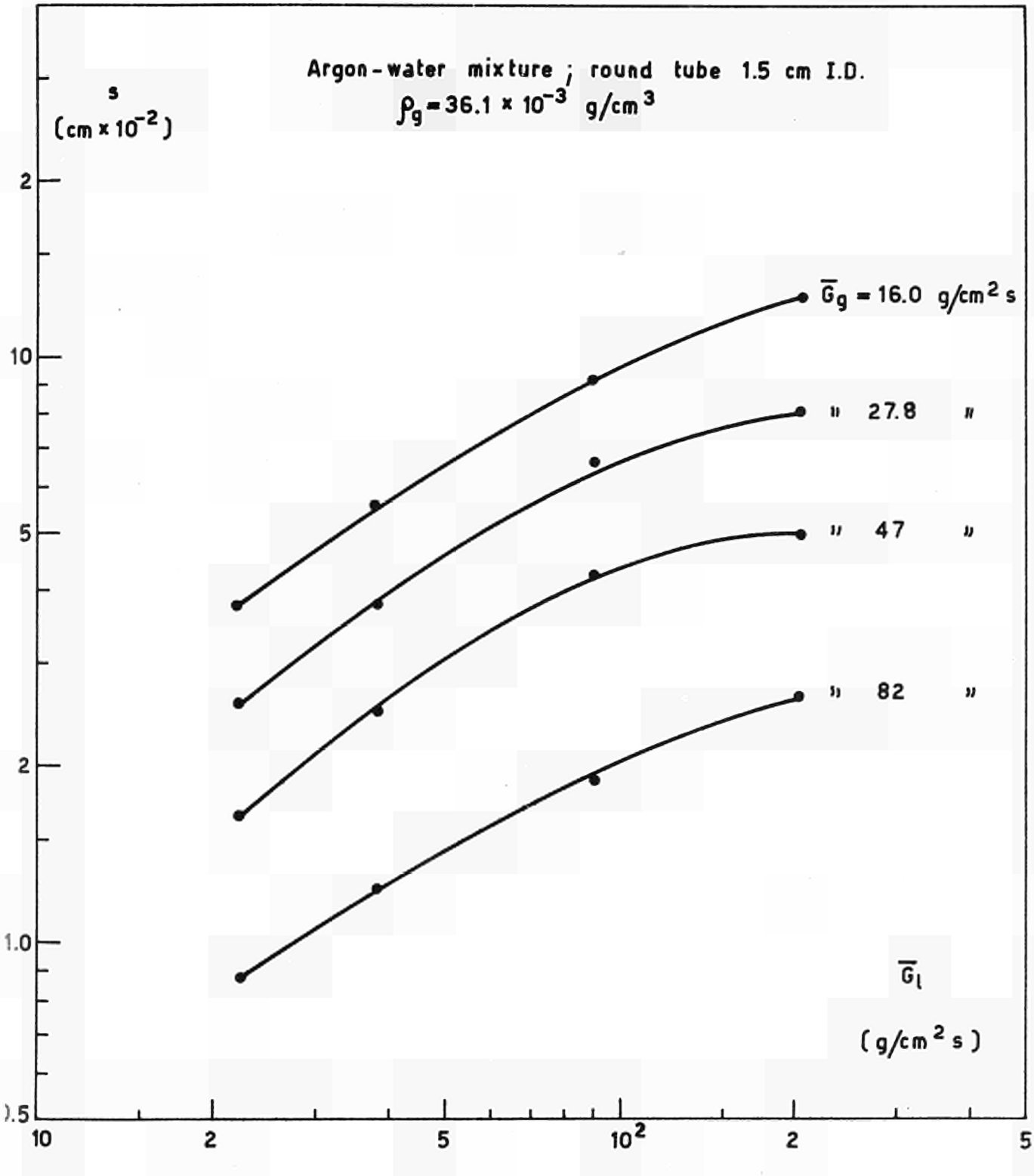

Fig.10 - Film thickness vs. average specific mass flowrate.

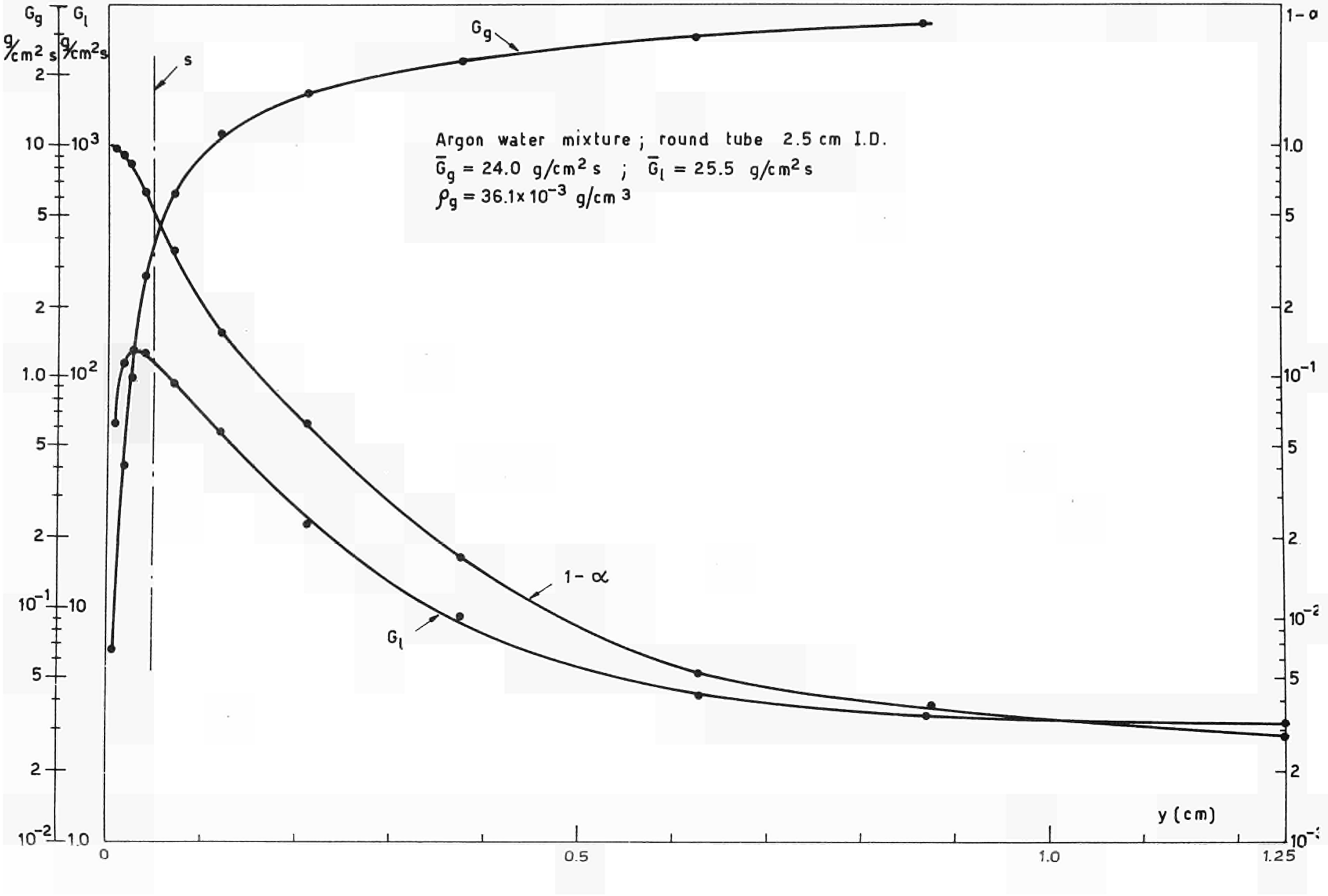
G_g g/cm² s
G_l g/cm² s
1 − α
s
G_g
Argon water mixture ; round tube 2.5 cm I.D.
$\bar{G}_g$ = 24.0 g/cm² s ; $\bar{G}_l$ = 25.5 g/cm² s
ρ_g = 36.1 x 10⁻³ g/cm³
1 − α
G_l
y (cm)
0
0.5
1.0
1.25

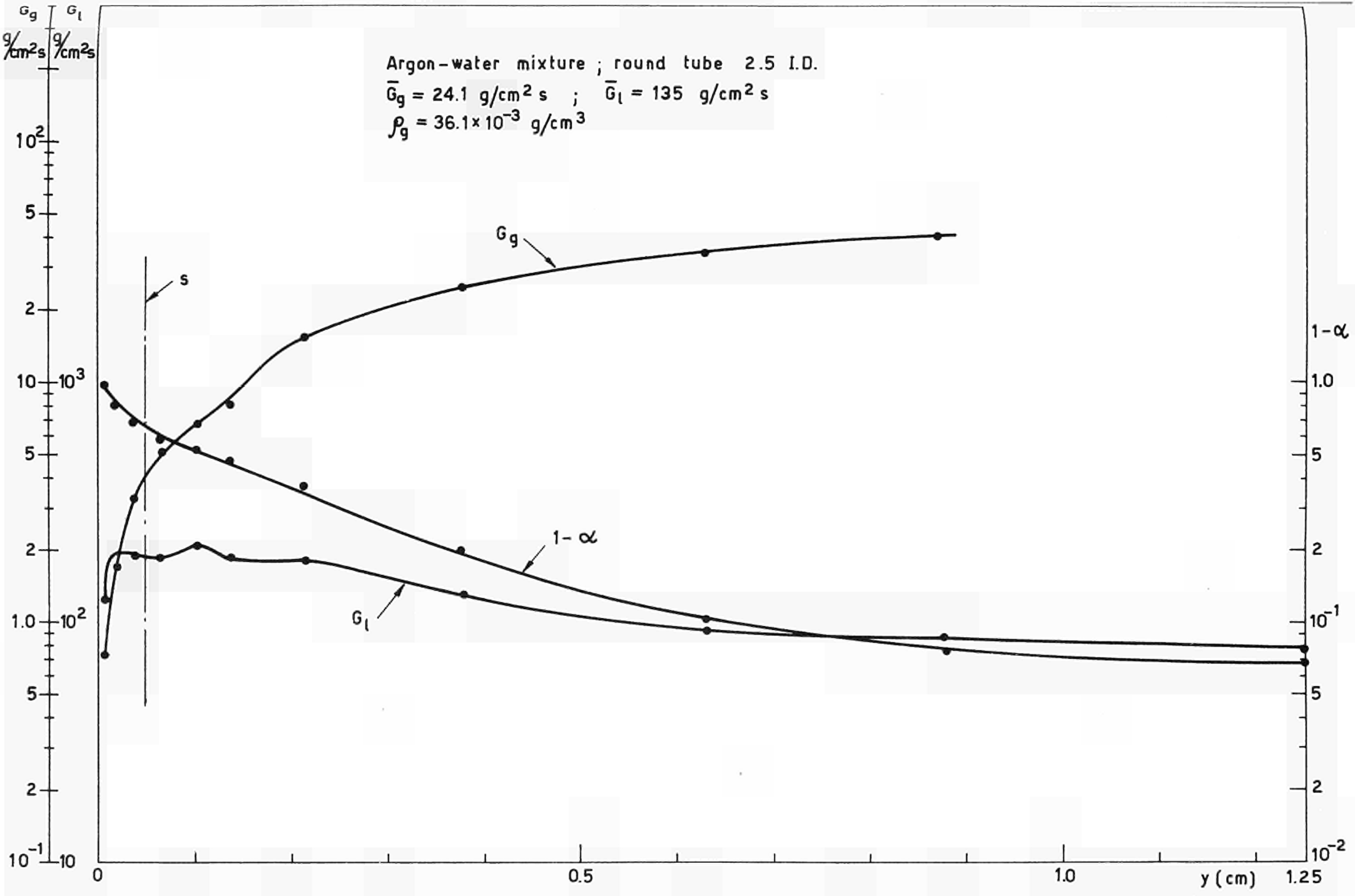

Fig.12 - Phase distribution and velocity profiles.

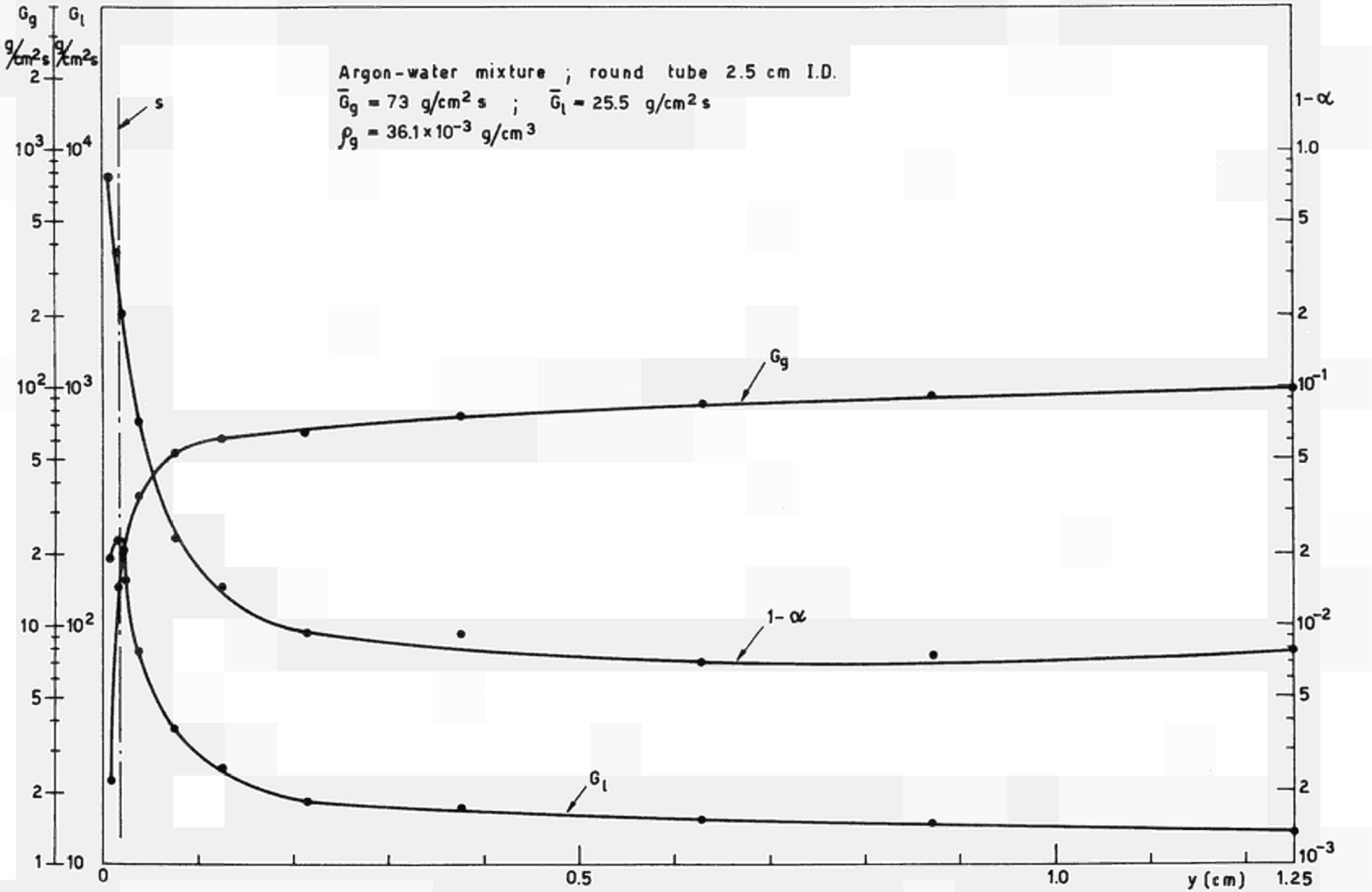

Fig.13 - Phase distribution and velocity profiles.

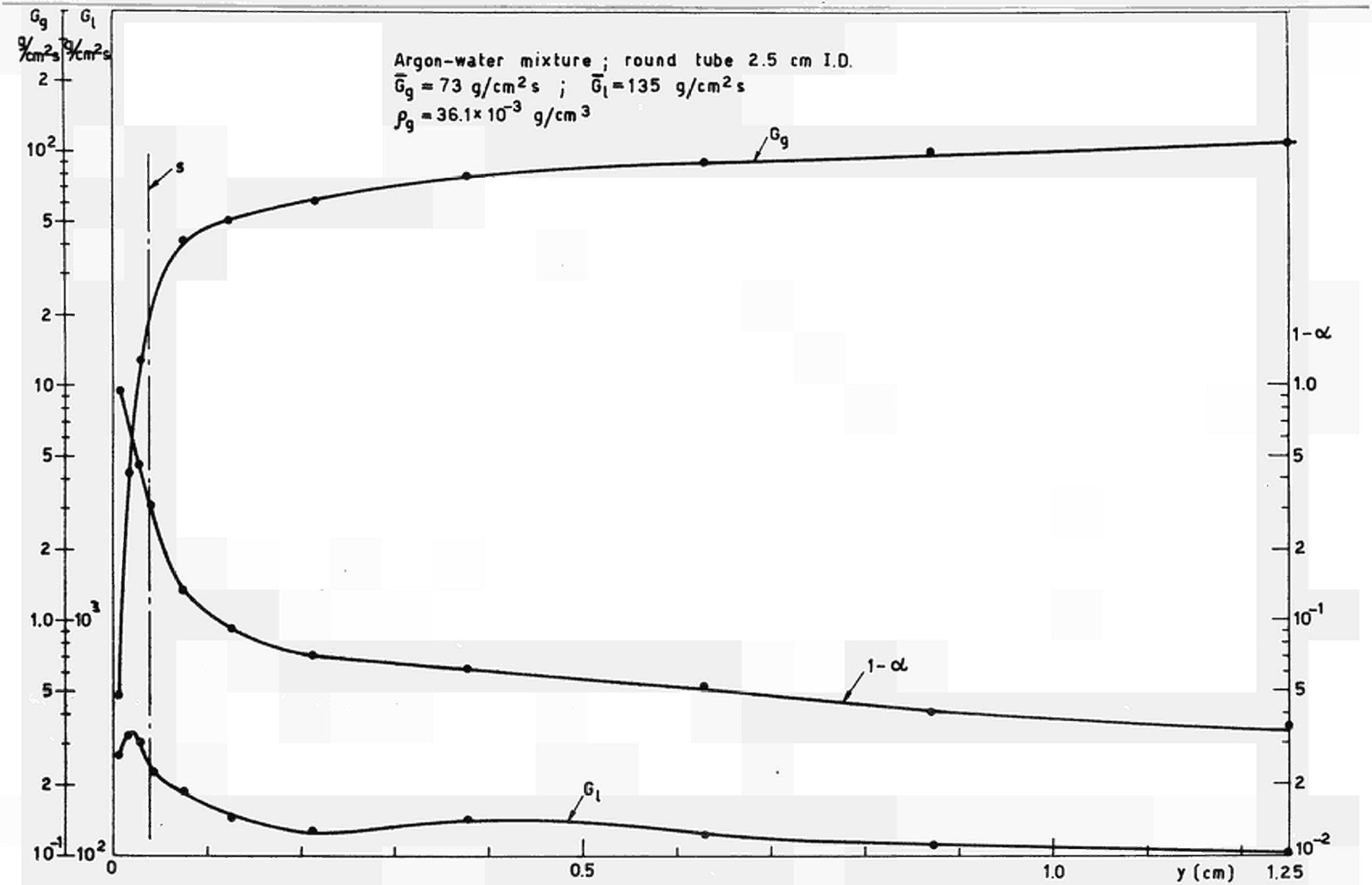

Fig.14 - Phase distribution and velocity profiles.

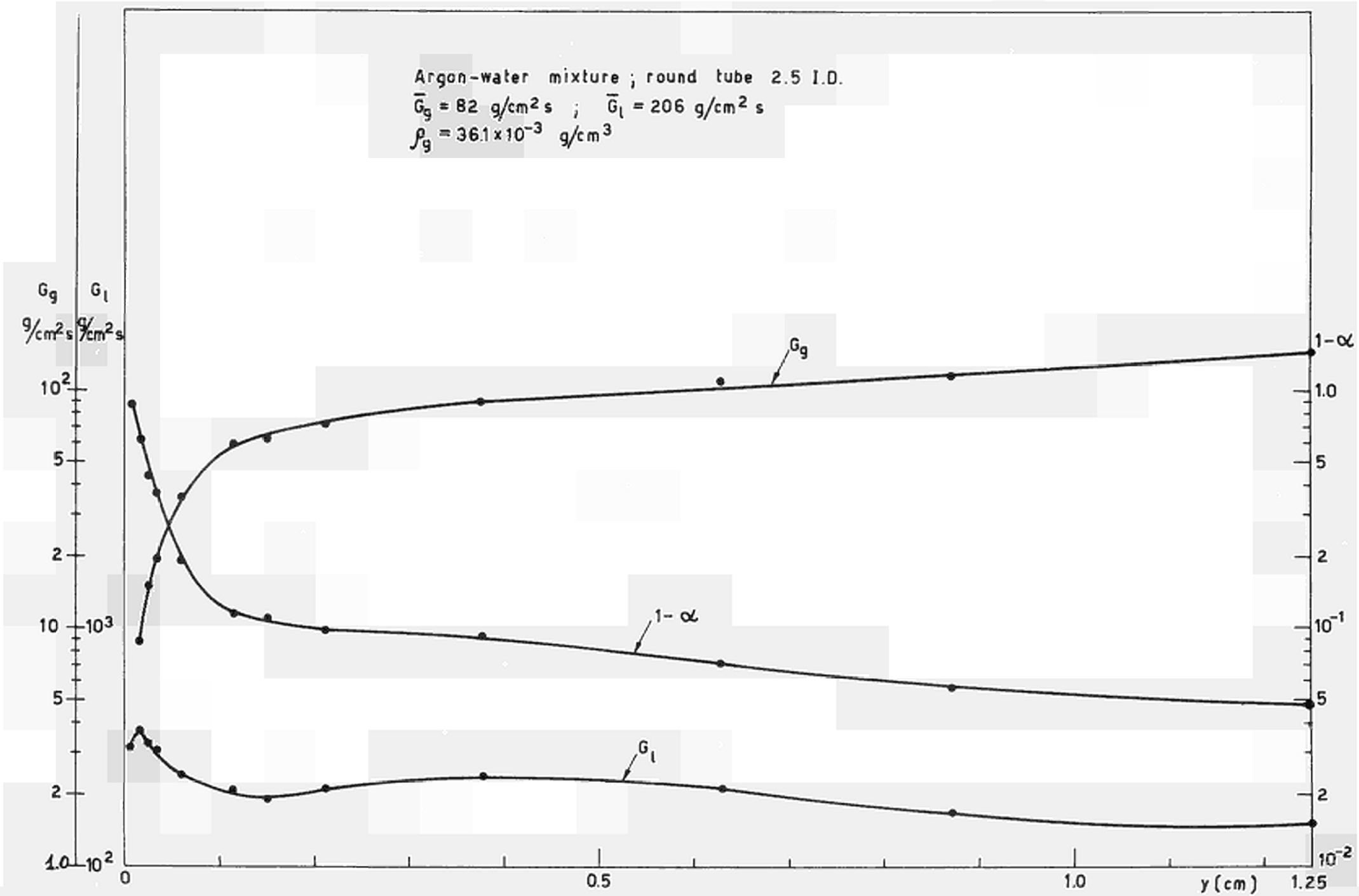

Fig.15 - Phase distribution and velocity profiles.

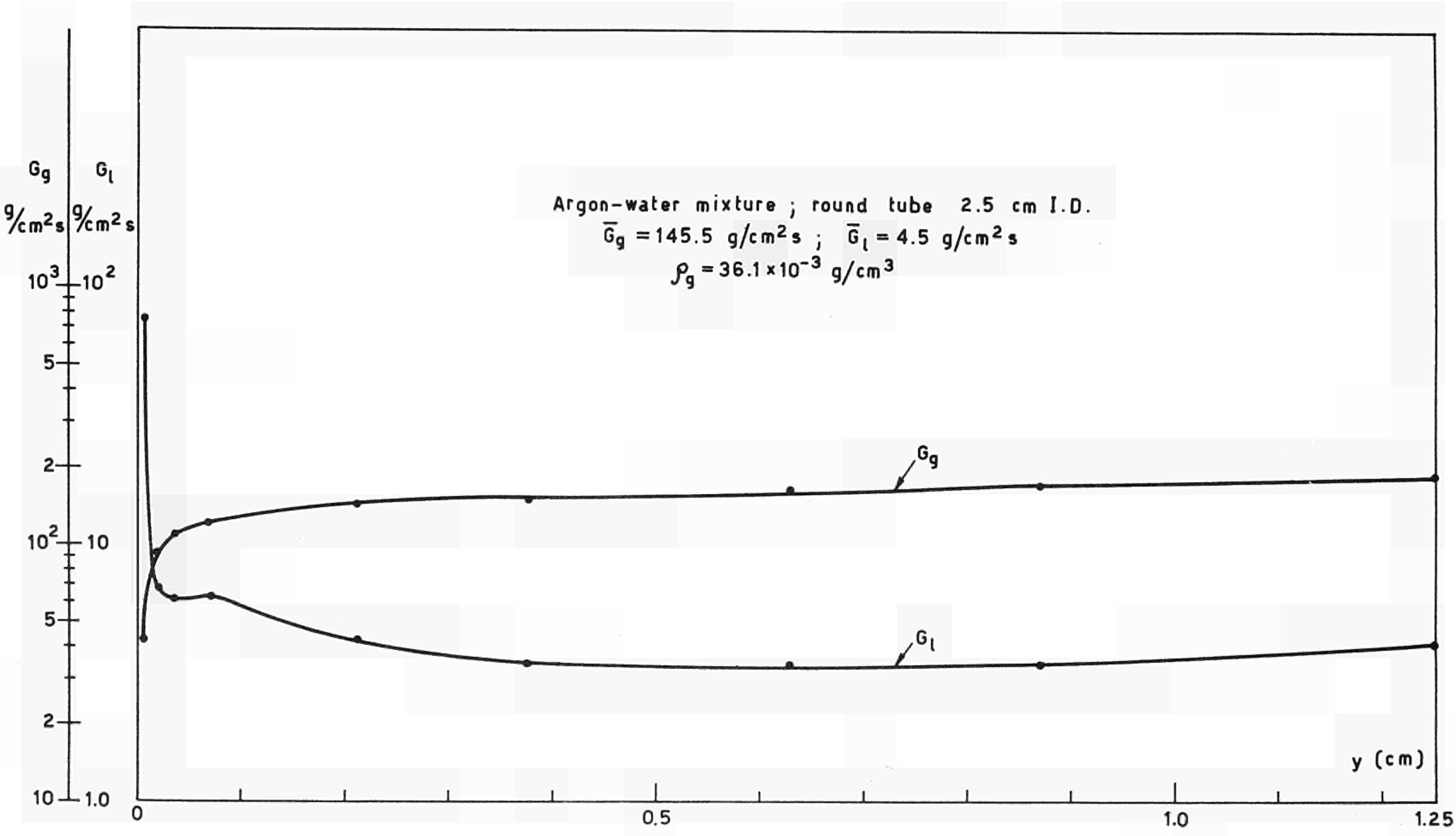

Fig. 16 - Phase distribution and velocity profiles.

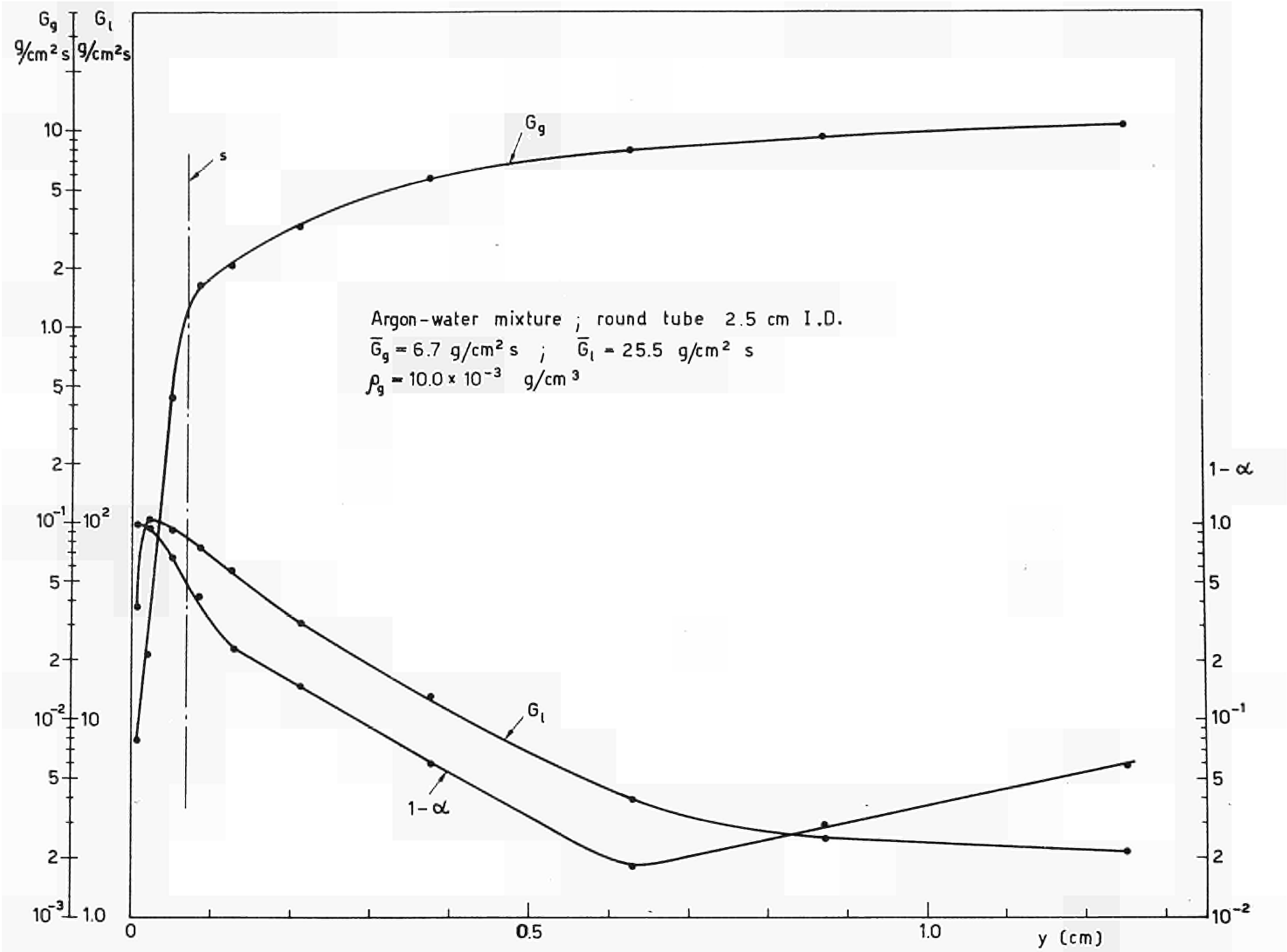

Fig.17 - Phase distribution and velocity profiles.

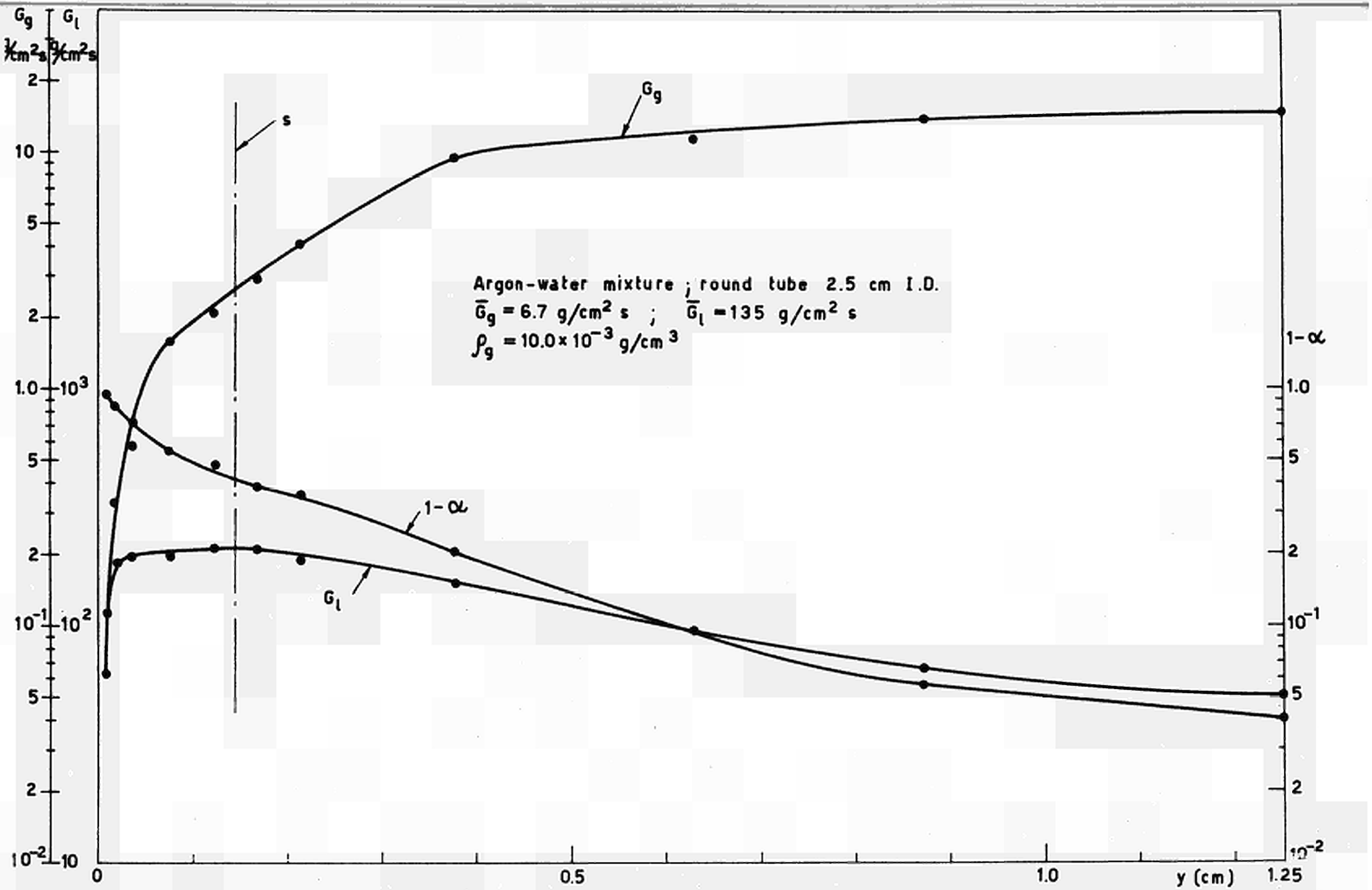

Fig. 18 - Phase distribution and velocity profiles.

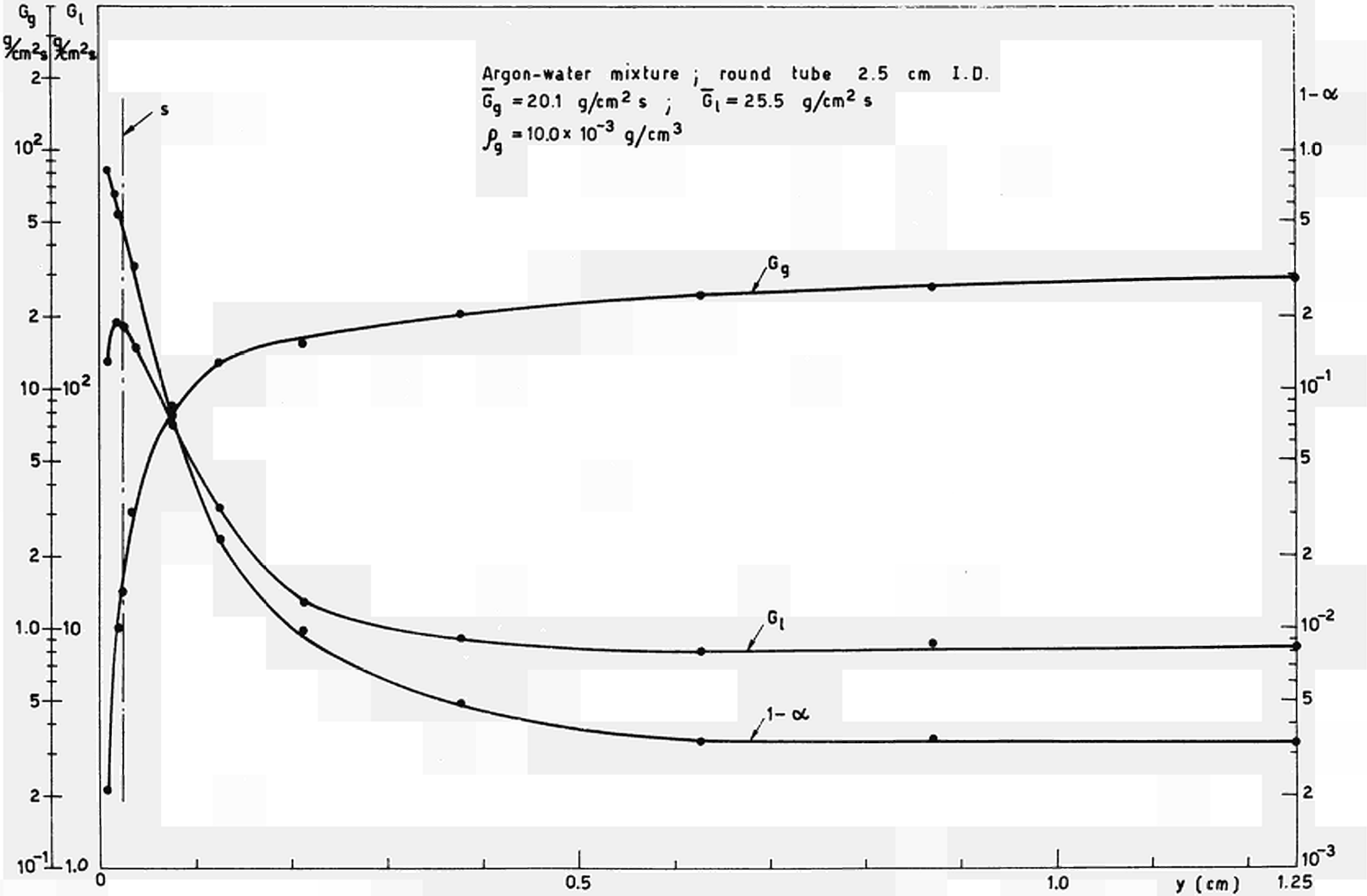

Fig. 19 - Phase distribution and velocity profiles.

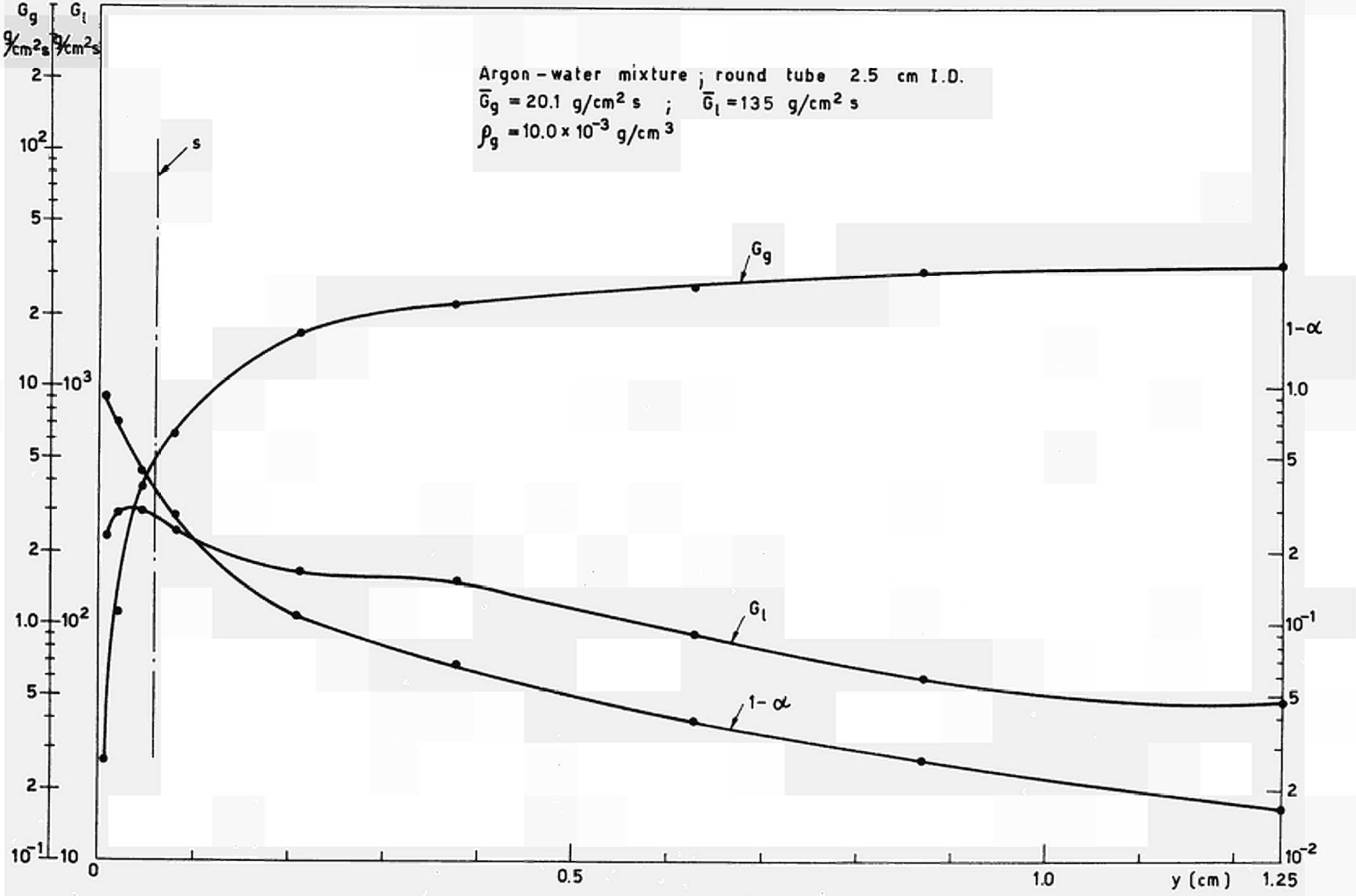

Fig.20 - Phase distribution and velocity profiles.

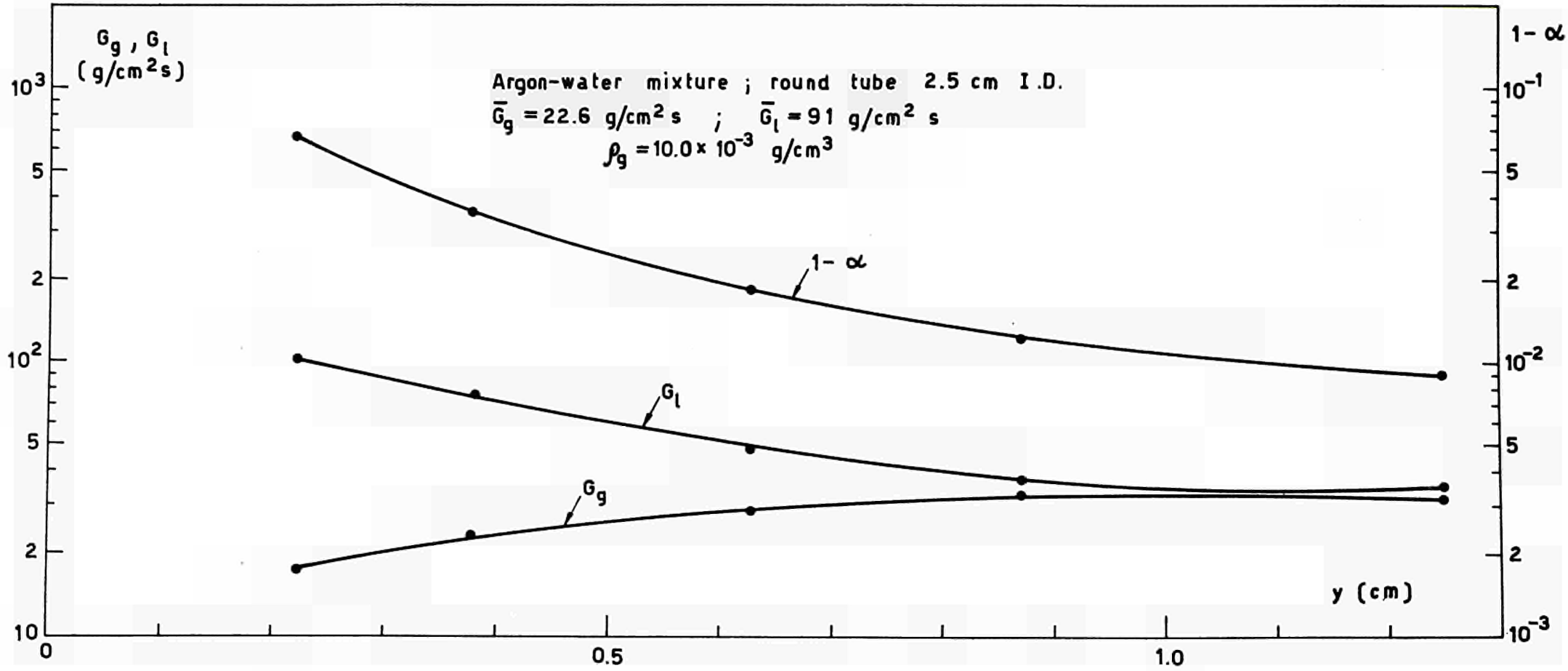

Fig.21 - Phase distribution and velocity profiles.

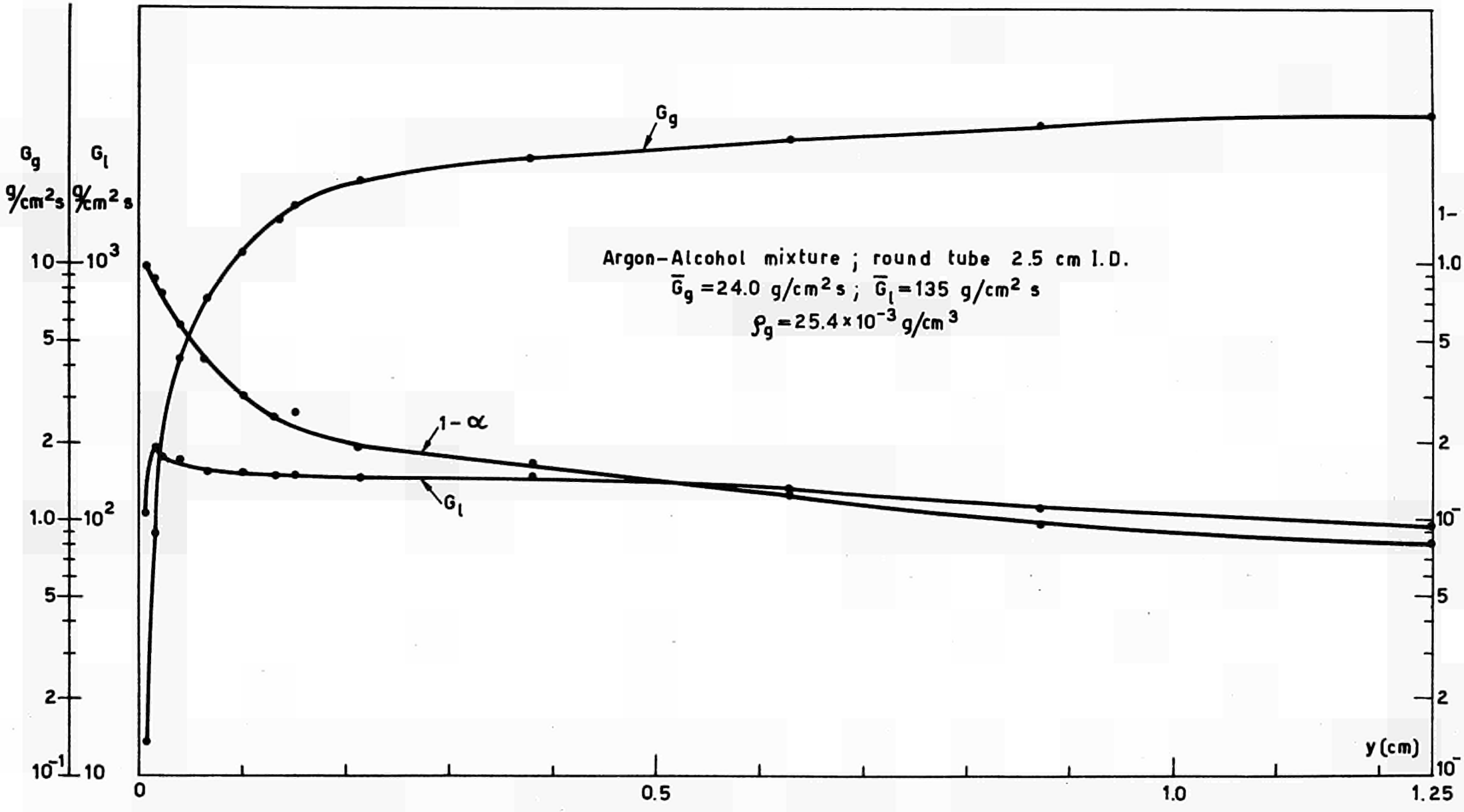

Fig. 22 - Phase distribution and velocity profiles.

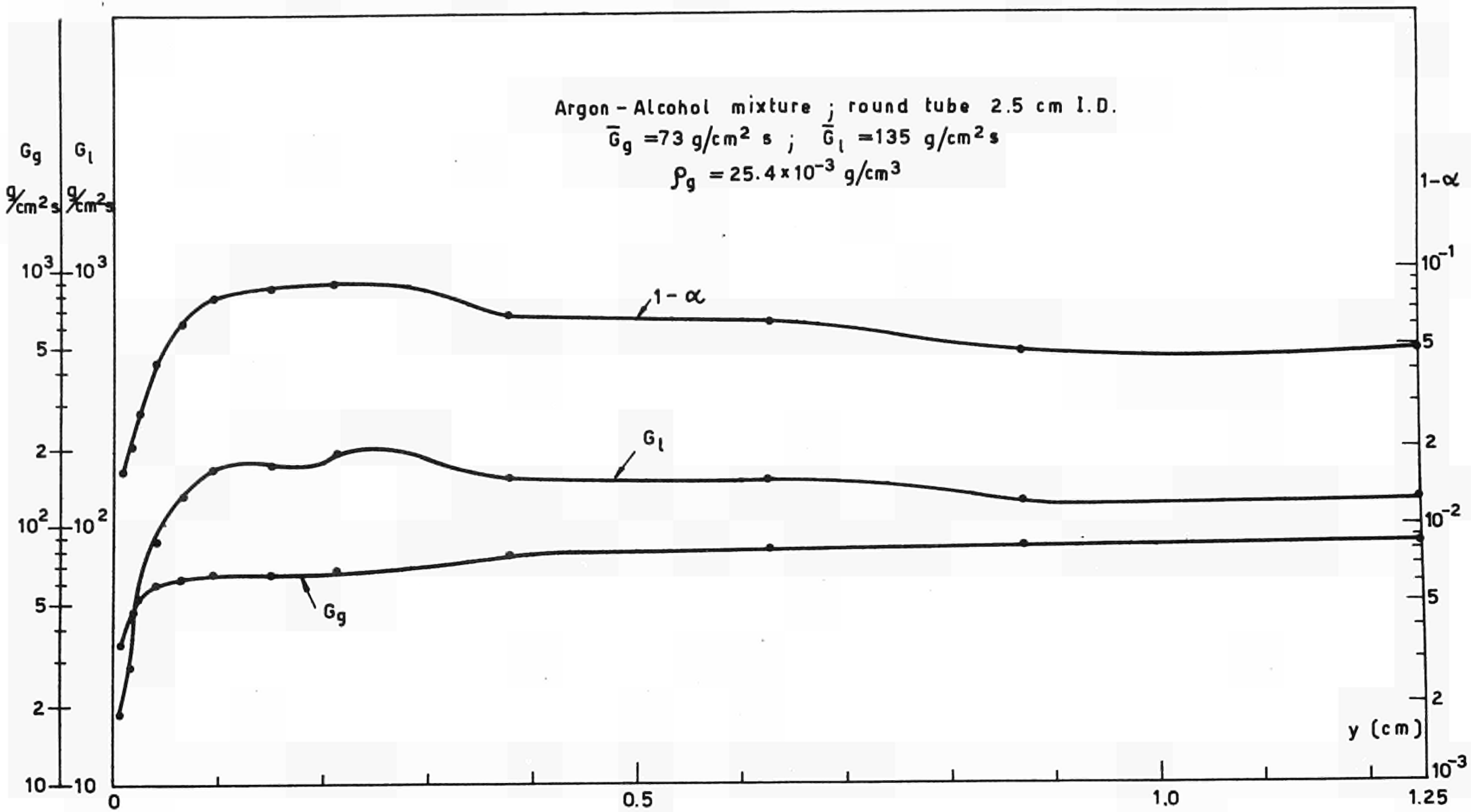

Fig.23 - Phase distribution and velocity profiles.

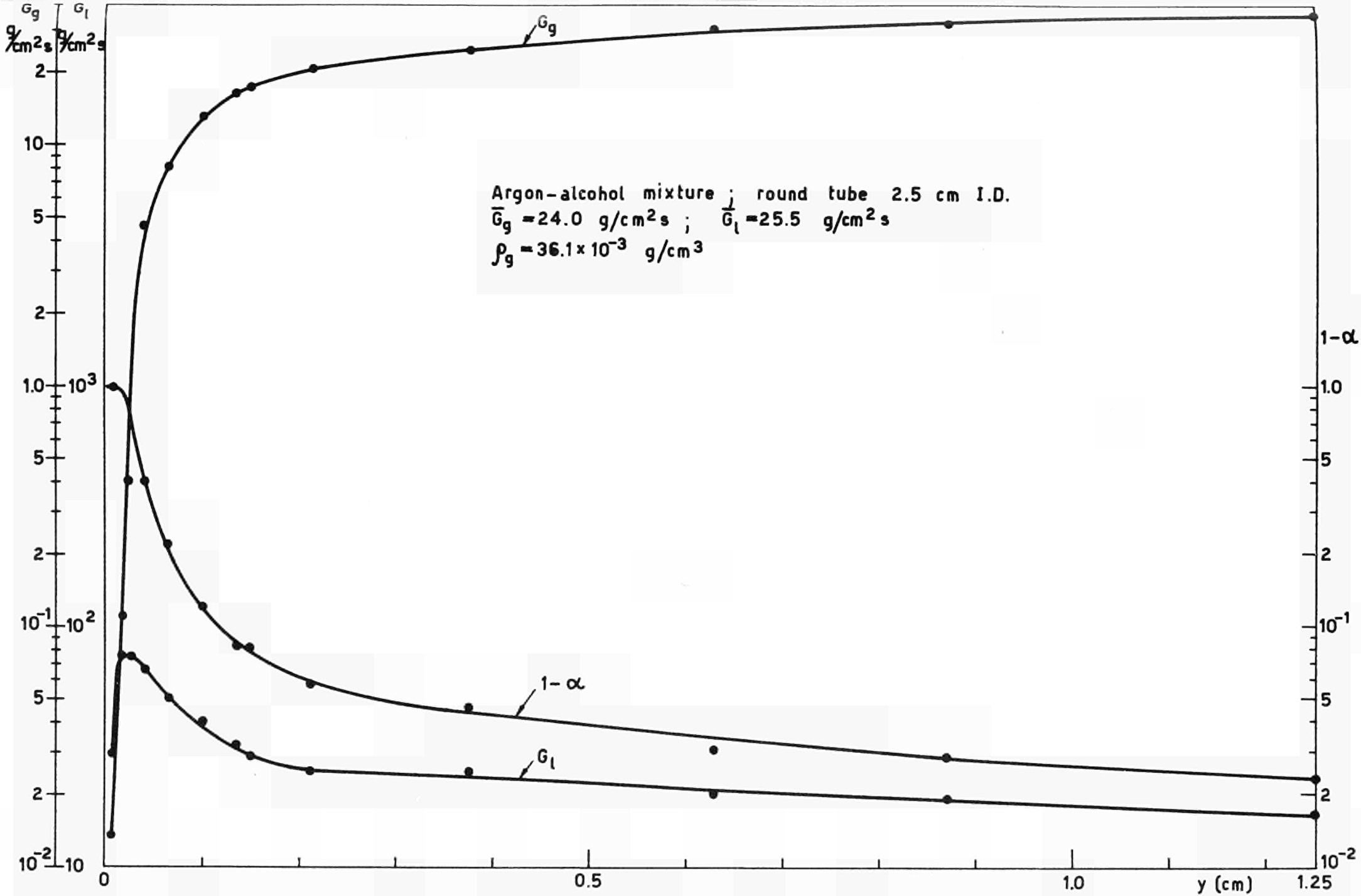

Fig. 24 - Phase distribution and velocity profiles.

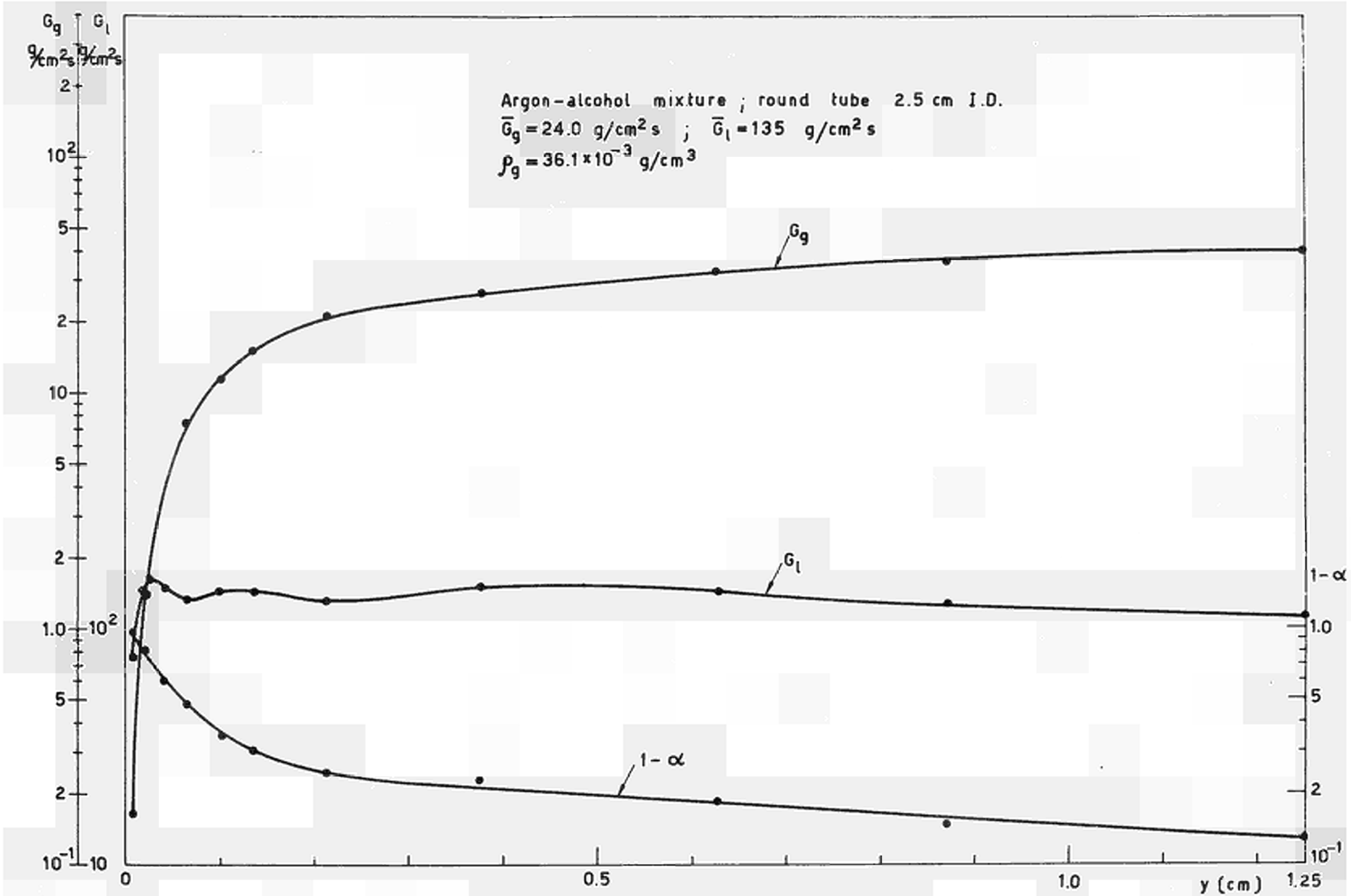

Fig.25 - Phase distribution and velocity profiles.

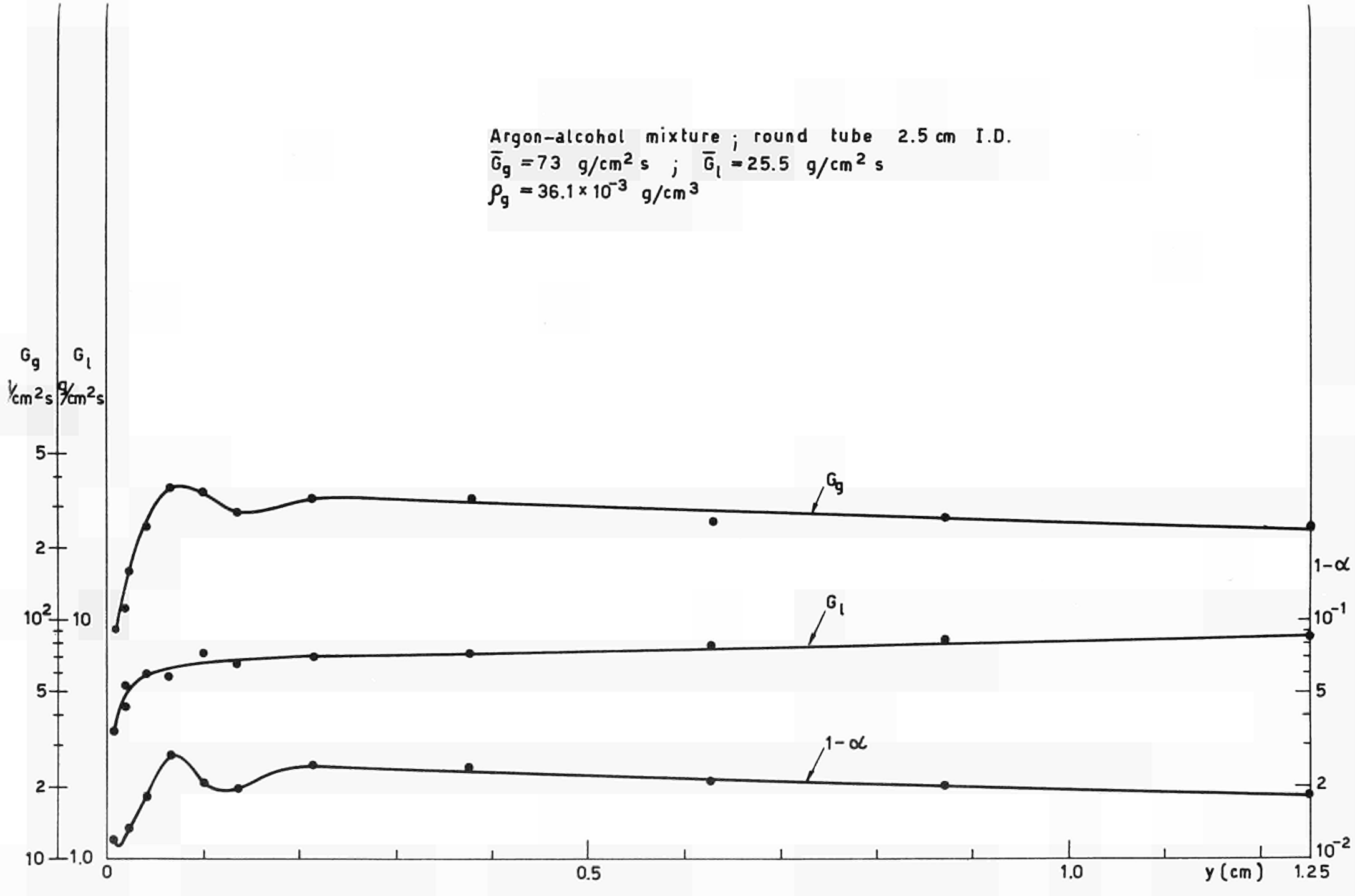

Fig.26 - Phase distribution and velocity profiles.

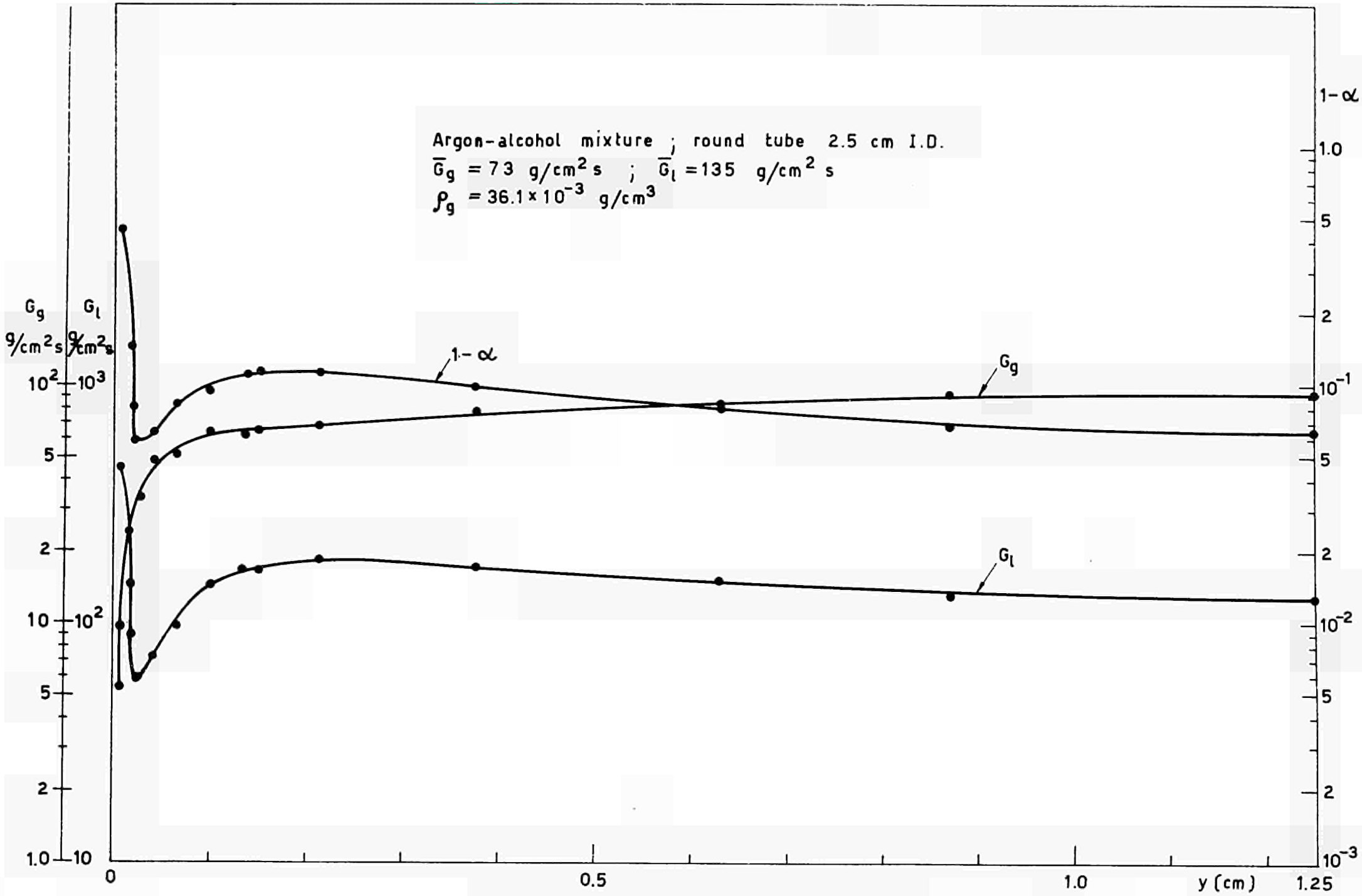

Fig.27 - Phase distribution and velocity profiles.

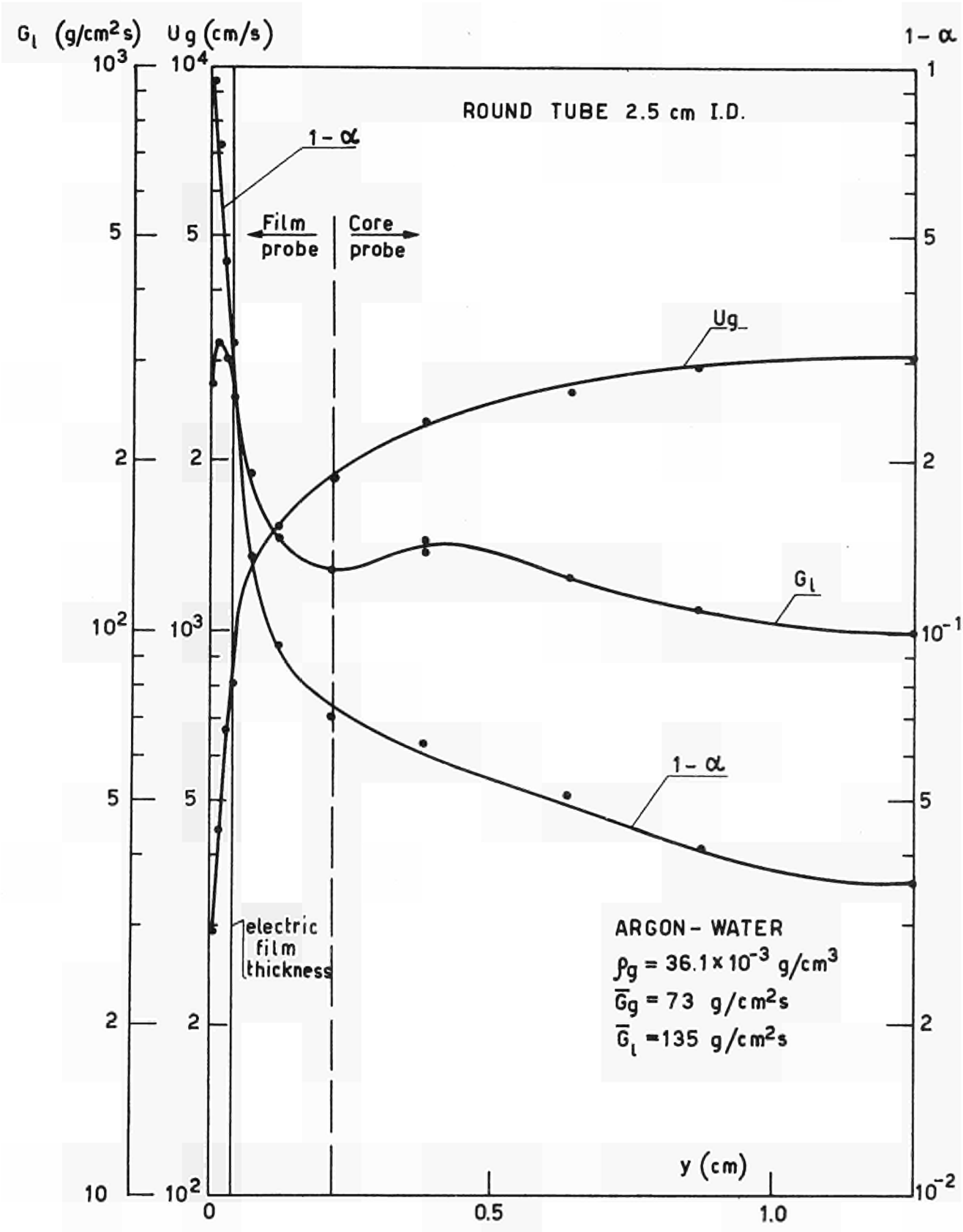

Fig.28 - Typical diagram of the local values of the liquid volume fraction the liquid specific mass flow rate and the gas velocity.

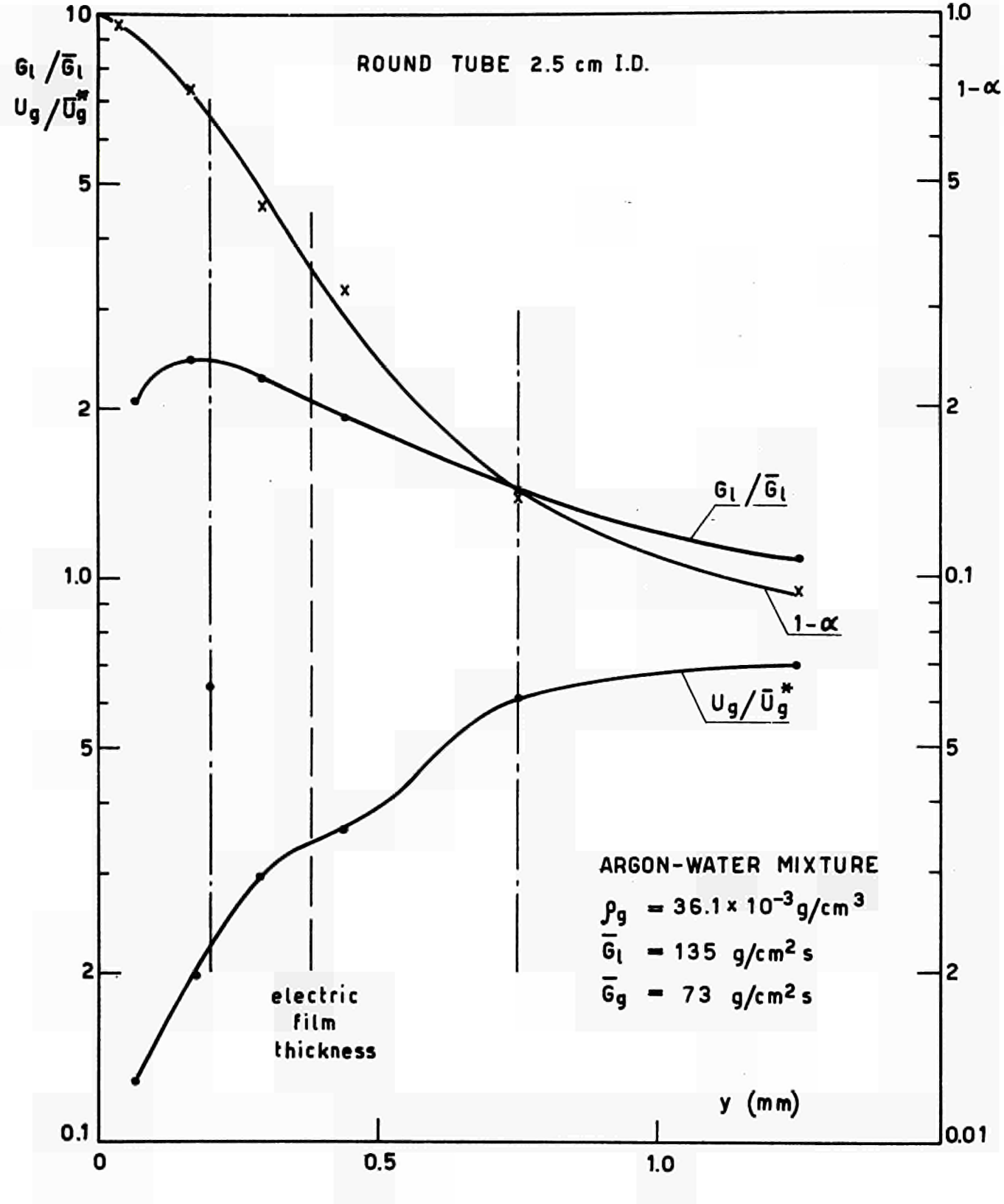

Fig. 29 - Typical diagram of the local liquid volume fraction, the liquid specific mass flow rate and the gas velocity in the region close to the wall.

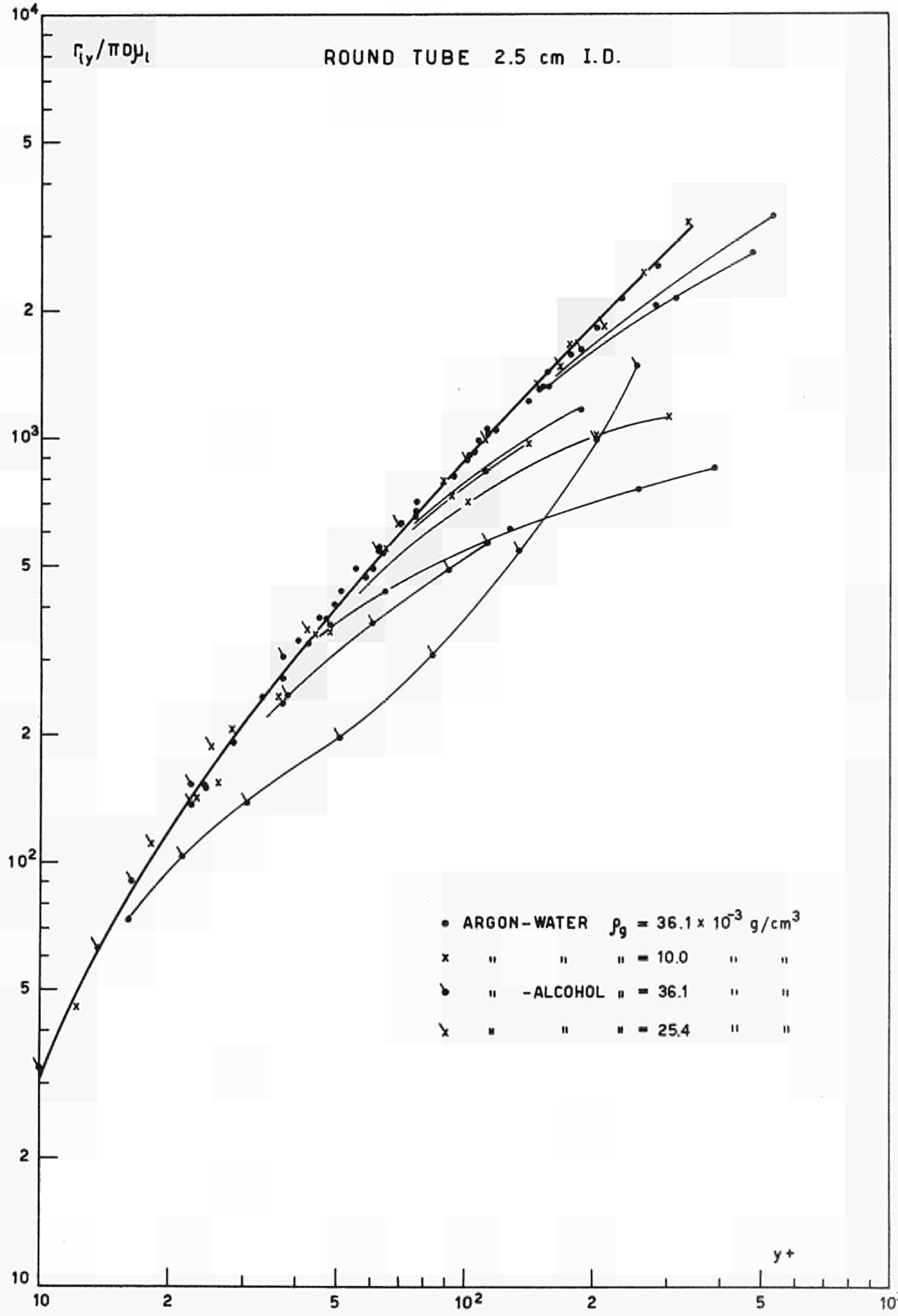

Fig.30 - Ratio of the liquid mass flow rate up to distance y from the wall to the quantity $\pi D \mu_l$, as a function of the dimensionless parameter y^+.

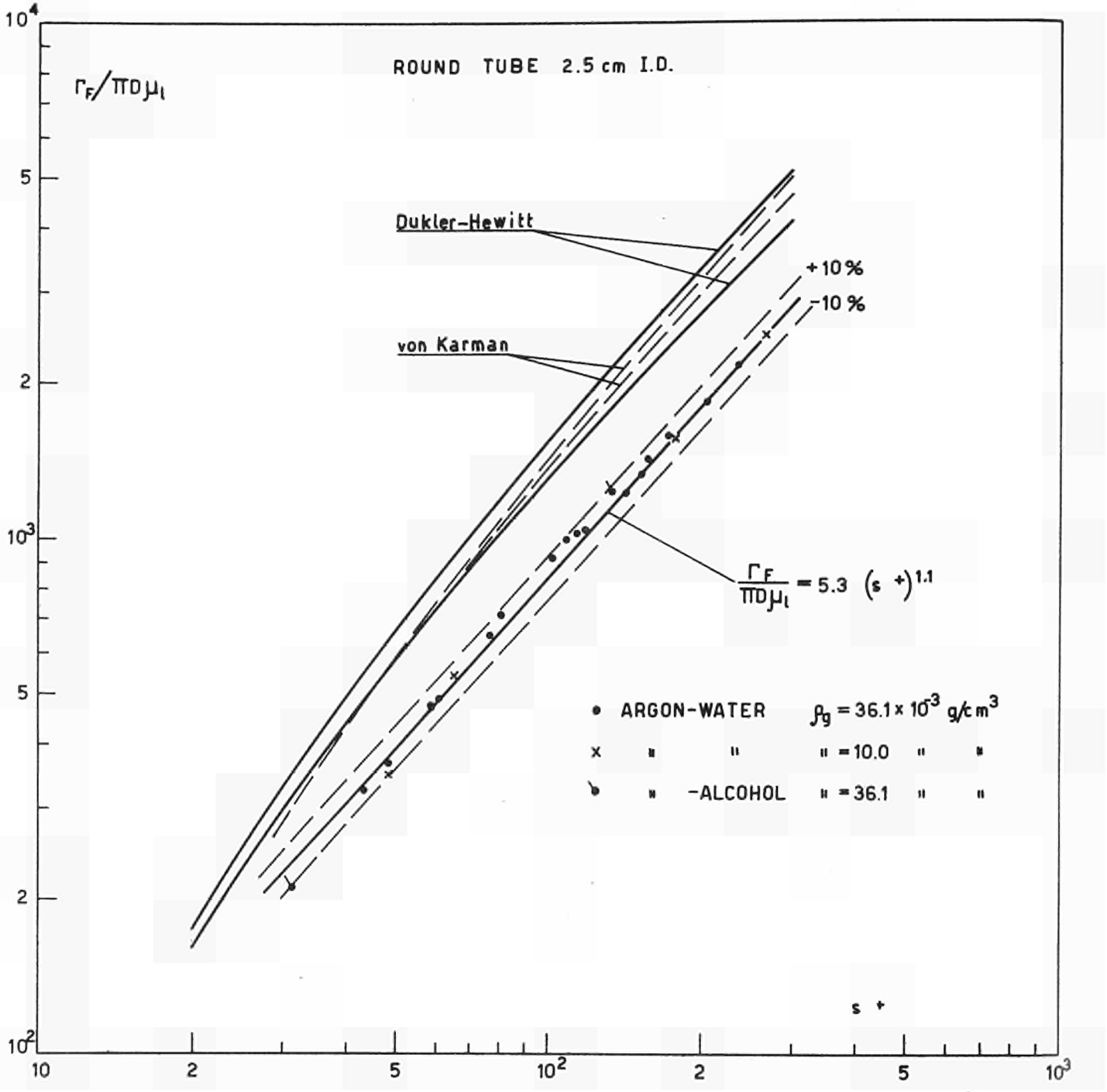

Fig.31 - Ratio of the liquid flow rate in the "film" (up to y = s) to the quantity π D μ_l, as a function of the dimensionless parameter s^+.

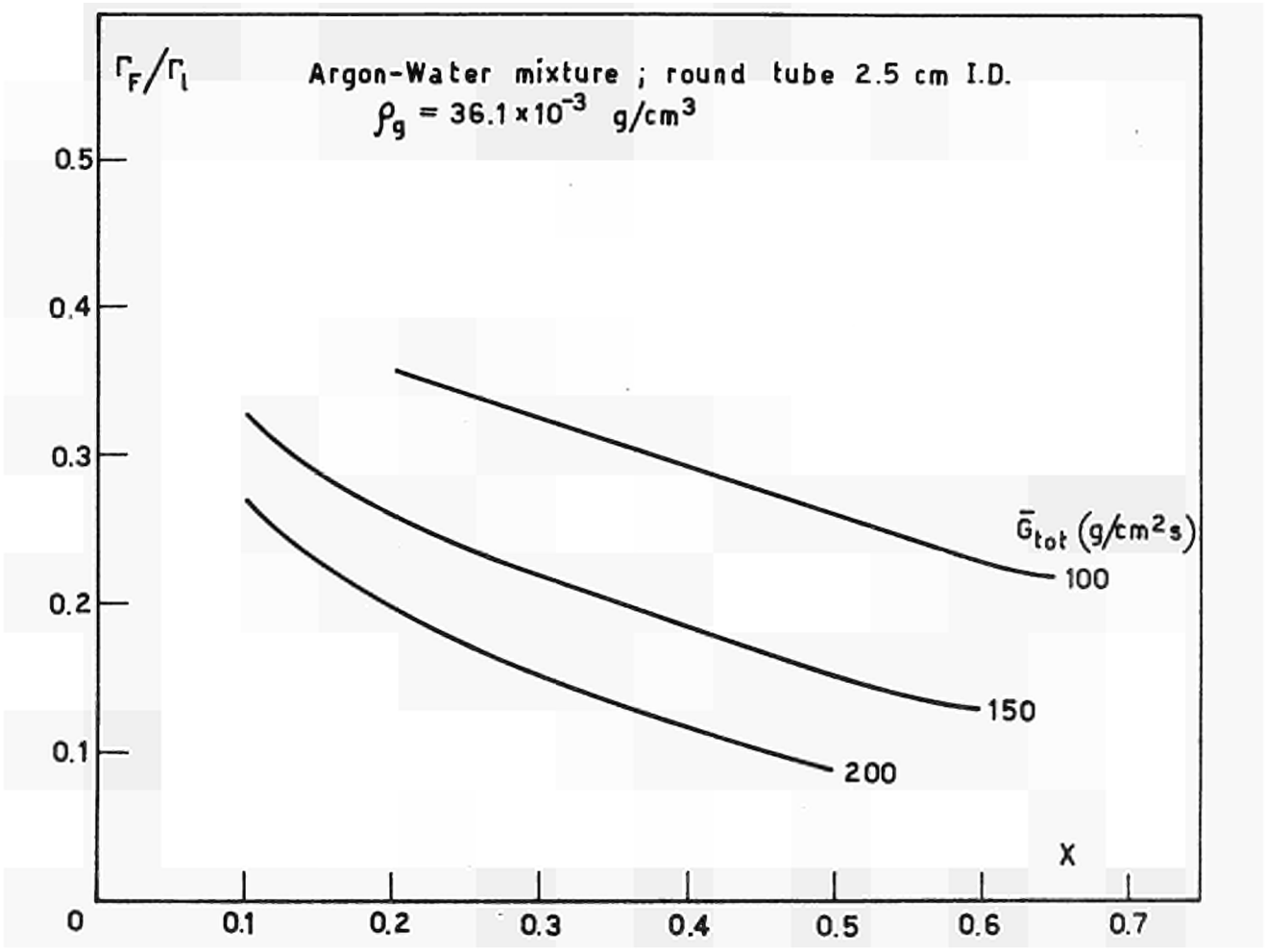

Fig.32 - Ratio of the "film" to the total liquid mass flow rate as a function of mass quality with total specific mass flow rate as a parameter.

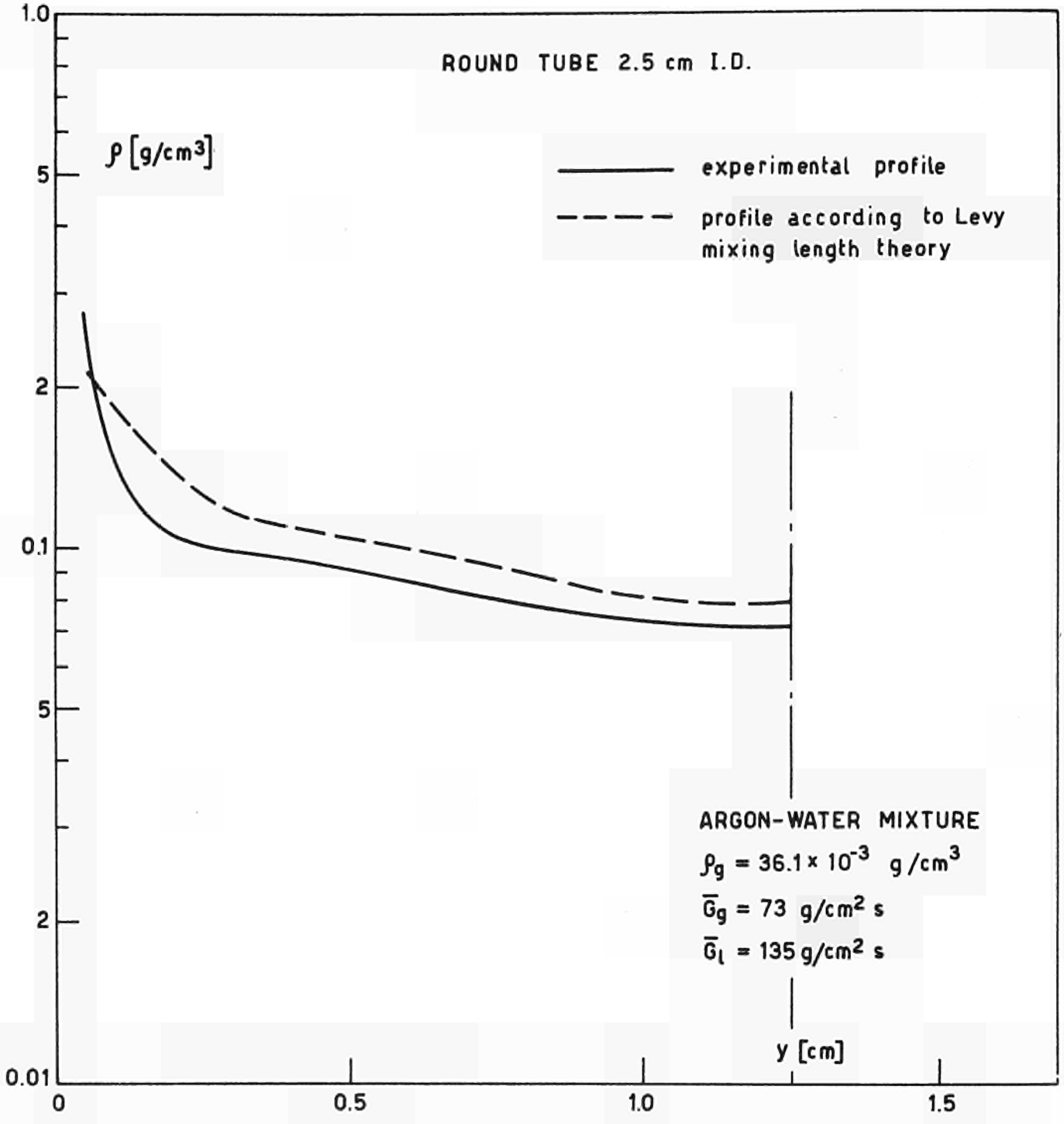

Fig. 33 - Comparison between the density profile as predicted by Levy mixing length theory and the experimental values.

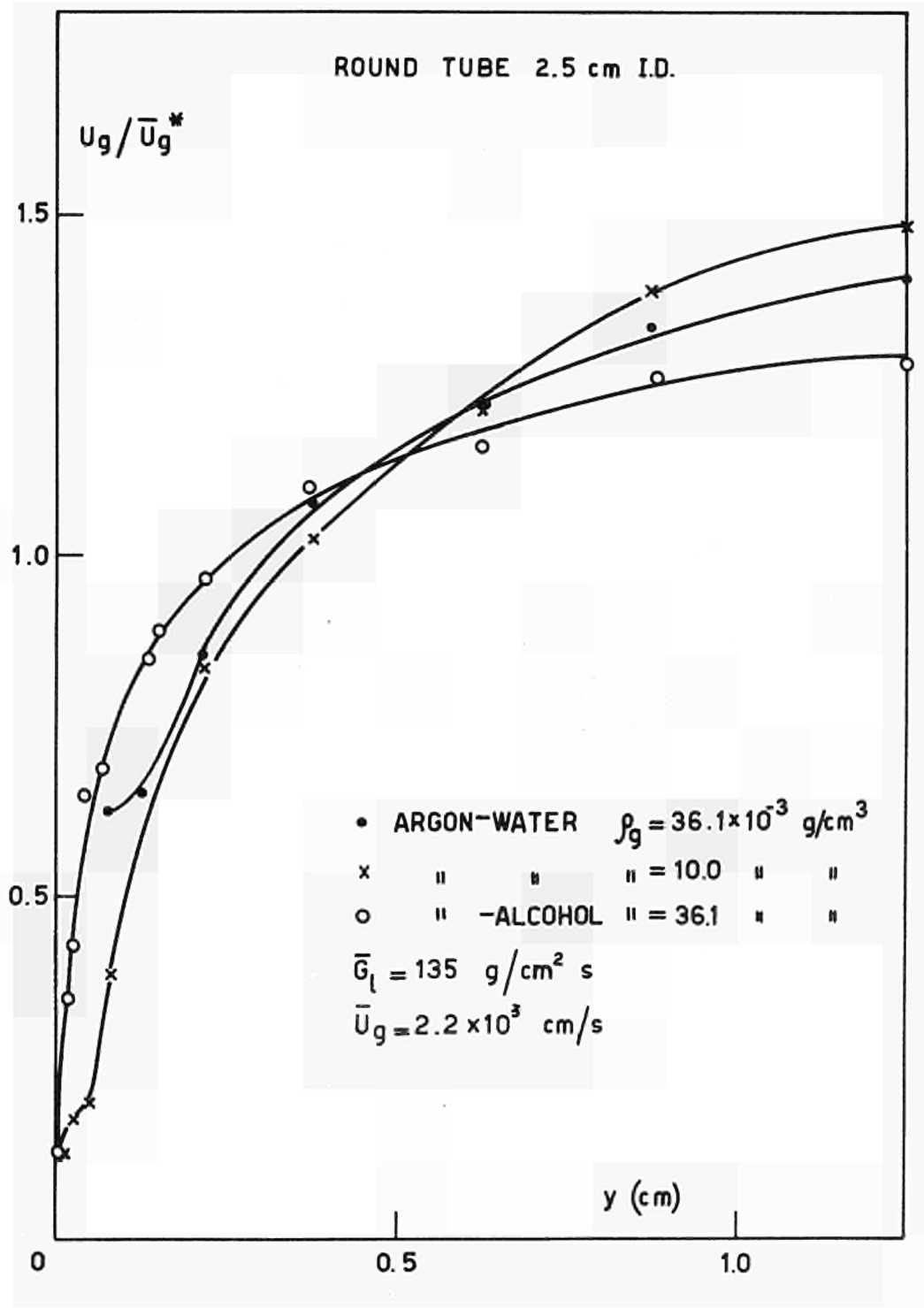

Fig. 34 - The influence of physical properties on the gas velocity profile on the core region.

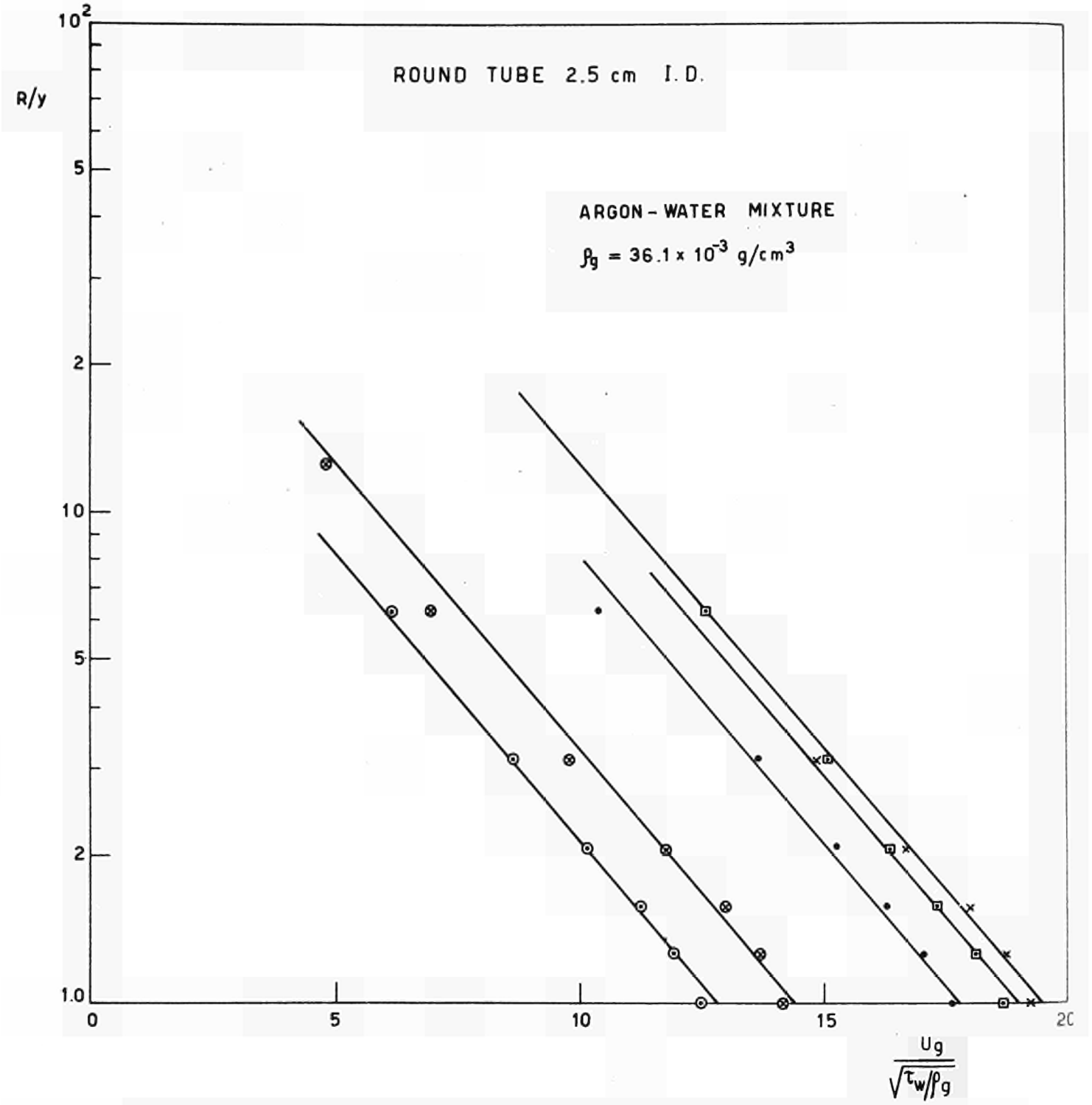

Fig.35 - Velocity deficiency law for gas phase in two-phase annular dispersed flow.

NOTICE TO THE READER

All Euratom reports are announced, as and when they are issued, in the monthly periodical **EURATOM INFORMATION,** edited by the Centre for Information and Documentation (CID). For subscription (1 year : US$ 15, £ 5.7) or free specimen copies please write to :

Handelsblatt GmbH
"Euratom Information"
Postfach 1102
D-4 Düsseldorf (Germany)

or

Office de vente des publications
des Communautés européennes
2, Place de Metz
Luxembourg

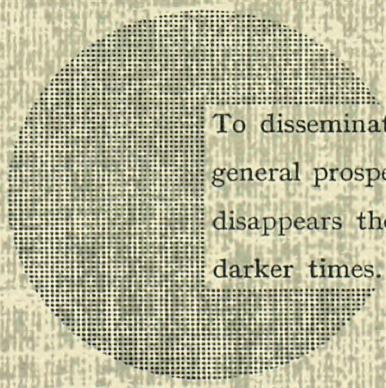

To disseminate knowledge is to disseminate prosperity — I mean general prosperity and not individual riches — and with prosperity disappears the greater part of the evil which is our heritage from darker times.

Alfred Nobel

SALES OFFICES

All Euratom reports are on sale at the offices listed below, at the prices given on the back of the front cover (when ordering, specify clearly the EUR number and the title of the report, which are shown on the front cover).

OFFICE CENTRAL DE VENTE DES PUBLICATIONS DES COMMUNAUTES EUROPEENNES
2, place de Metz, Luxembourg (Compte chèque postal Nº 191-90)

BELGIQUE — BELGIË
MONITEUR BELGE
40-42, rue de Louvain - Bruxelles
BELGISCH STAATSBLAD
Leuvenseweg 40-42, - Brussel

DEUTSCHLAND
BUNDESANZEIGER
Postfach - Köln 1

FRANCE
SERVICE DE VENTE EN FRANCE DES PUBLICATIONS DES COMMUNAUTES EUROPEENNES
26, rue Desaix - Paris 15e

ITALIA
LIBRERIA DELLO STATO
Piazza G. Verdi, 10 - Roma

LUXEMBOURG
OFFICE CENTRAL DE VENTE DES PUBLICATIONS DES COMMUNAUTES EUROPEENNES
9, rue Goethe - Luxembourg

NEDERLAND
STAATSDRUKKERIJ
Christoffel Plantijnstraat - Den Haag

UNITED KINGDOM
H. M. STATIONERY OFFICE
P. O. Box 569 - London S.E.1

EURATOM — C.I.D.
51-53, rue Belliard
Bruxelles (Belgique)

CDNA03759ENC